AGU PUBLICATIONS

JGR

Journal of Geophysical Research: Solid Earth

RESEARCH ARTICLE
10.1002/2017JB014082

Key Points:
- A new crustal seismic model is constructed for Tolbachik and adjacent volcanoes
- Seismicity beneath Klyuchevskoy reflects a straight conduit that brings magma directly from the mantle
- The Bezymianny volcano is fed through separating felsic magma and volatiles from midcrustal sources

Correspondence to:
I. Koulakov,
koulakoviy@ipgg.sbras.ru

Citation:
Koulakov, I., et al. (2017), Three different types of plumbing system beneath the neighboring active volcanoes of Tolbachik, Bezymianny, and Klyuchevskoy in Kamchatka, *J. Geophys. Res. Solid Earth*, *122*, doi:10.1002/2017JB014082.

Received 8 FEB 2017
Accepted 13 APR 2017
Accepted article online 20 APR 2017

Three different types of plumbing system beneath the neighboring active volcanoes of Tolbachik, Bezymianny, and Klyuchevskoy in Kamchatka

Ivan Koulakov[1,2], Ilyas Abkadyrov[3], Nassir Al Arifi[4], Evgeny Deev[1,2], Svetlana Droznina[5], Evgeny I. Gordeev[3], Andrey Jakovlev[1], Sami El Khrepy[4,6], Roman I. Kulakov[7], Yulia Kugaenko[5], Anzhelika Novgorodova[1], Sergey Senyukov[5], Nikolay Shapiro[3,8], Tatyana Stupina[1], and Michael West[9]

[1]Department of Geophysics, Trofimuk Institute of Petroleum Geology and Geophysics SB RAS, Novosibirsk, Russia, [2]Department of Geology and Geophysics, Novosibirsk State University, Novosibirsk, Russia, [3]Institute of Volcanology and Seismology FEB RAS, Petropavlovsk-Kamchatsky, Russia, [4]King Saud University, Riyadh, Saudi Arabia, [5]Kamchatkan Branch of Geophysical Survey RAS Piip Boulevard, Petropavlovsk-Kamchatsky, Russia, [6]Department of Geophysics, National Research Institute of Astronomy and Geophysics, Helwan, Egypt, [7]Geology Department, Moscow State University, Moscow, Russia, [8]Institut de Physique du Globe de Paris, Sorbonne Paris Cité, CNRS (UMR 7154), Paris, France, [9]Geophysical Institute, University of Alaska Fairbanks, Fairbanks, Alaska, USA

Abstract The Klyuchevskoy group of volcanoes (KGV) in Kamchatka includes three presently active volcanoes (Klyuchevskoy, Bezymianny, and Tolbachik) located close together in an area of approximately 50 × 80 km. These three volcanoes have completely different compositions and eruption styles from each other. We have analyzed new data recorded by a temporary seismic network consisting of 22 seismic stations operated within the area of Tolbachik in 2014–2015 in conjunction with the data from the permanent network and the temporary PIRE network deployed at the Bezymianny volcano in 2009. The arrival times of the *P* and *S* waves were inverted using a local earthquake tomography algorithm to derive 3-D seismic models of the crust beneath the KGV as well as accurate seismicity locations. High-resolution structures beneath the Tolbachik volcanic complex were identified for the first time in this study. The tomography results reveal three different types of feeding system for the main KGV volcanoes. The basaltic lavas of the Klyuchevskoy volcano are supplied directly from a reservoir at a depth of 25–30 km through a nearly vertical pipe-shaped conduit. The explosive Bezymianny volcano is fed through a dispersed system of crustal reservoirs where a lighter felsic material separates from the mafic component and ascends to the upper crust to form andesitic magma sources. For Tolbachik, low-viscosity volatile-saturated basalts ascend from two deep reservoirs following a system of fractures in the crust associated with the intersections of regional faults.

Plain Language Summary The Klyuchevskoy group of volcanoes (KGV) in Kamchatka includes three presently active volcanoes (Klyuchevskoy, Bezymianny, and Tolbachik) located close together in an area of approximately 50 × 80 km. These three volcanoes are among the most active volcanoes in the world, and they have completely different compositions and eruption styles from each other. We have analyzed new data recorded by a temporary seismic network consisting of 22 seismic stations installed within the area of Tolbachik in 2014–2015 in harsh natural conditions. Based on these data, we have derived high-resolution structures beneath the Tolbachik volcanic complex and surrounding areas. The tomography results reveal three different types of feeding system for the main KGV volcanoes. The basaltic lavas of the Klyuchevskoy volcano are supplied directly from a reservoir at a depth of 25–30 km through a nearly vertical pipe-shaped conduit. The explosive Bezymianny volcano is fed through a dispersed system of crustal reservoirs where a lighter felsic material separates from the mafic component and ascends to the upper crust to form andesitic magma sources. For Tolbachik, low-viscosity volatile-saturated basalts ascend from two deep reservoirs following a system of fractures in the crust associated with the intersections of regional faults.

1. Introduction

The Klyuchevskoy group of volcanoes (KGV) in Kamchatka, Russia is a unique volcanic system with remarkable diversity and intense recent eruptions [e.g., *Laverov*, 2005; *Ponomareva et al.*, 2007]. Among the dozen KGV volcanoes within an 80 × 50 km area (Figure 1), three are among the world's most active volcanoes.

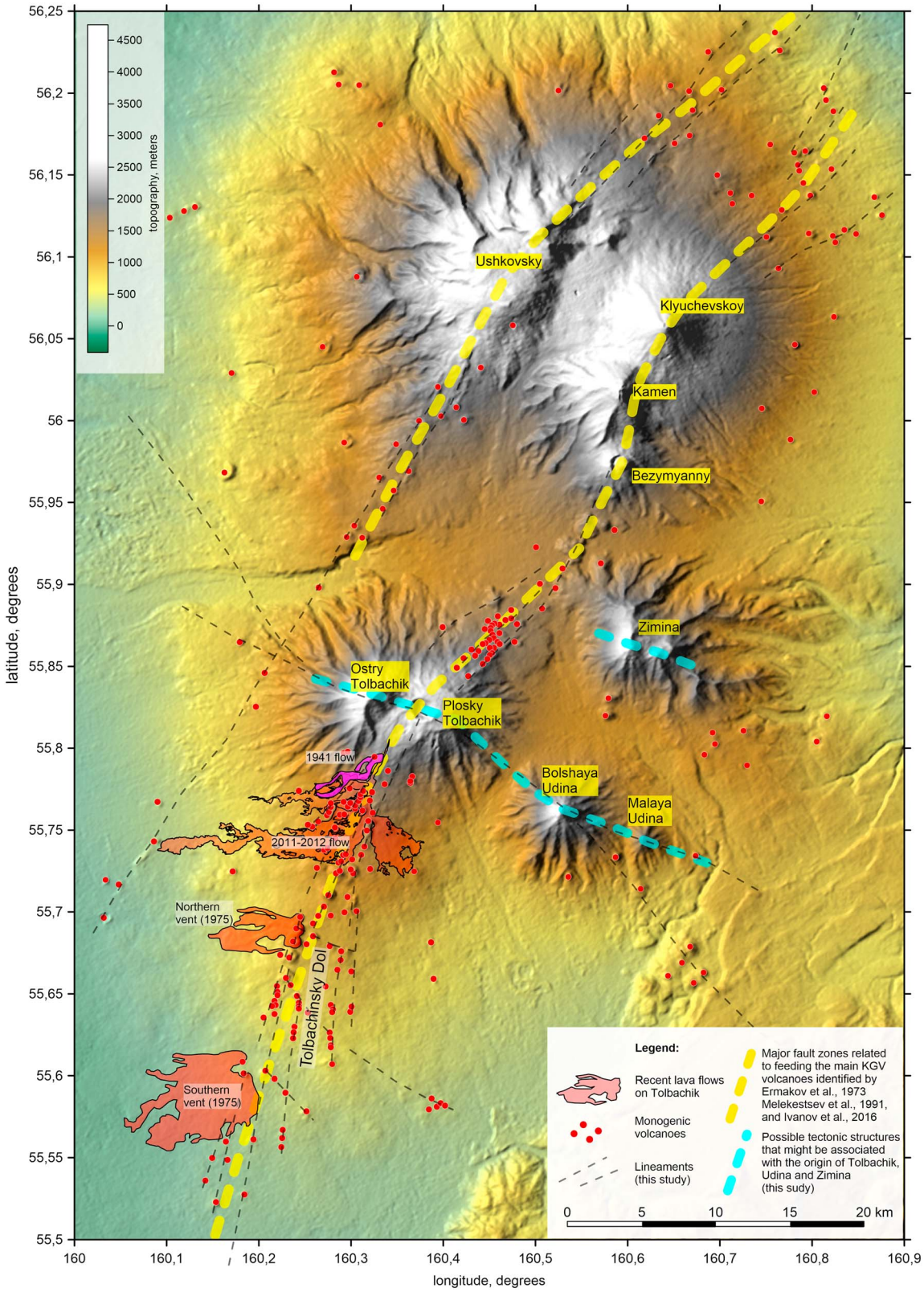

Figure 1. Relief map of the Klyuchevskoy volcano group (from www.marine-geo.org) with the main volcanic structures and lineaments indicated. Monogenetic volcanoes and lava flows of Tolbachik are from *Churikova et al.* [2015]; other monogenetic volcanoes are identified based on topographic features. The blue and yellow bold, dotted lines depict major fault zones that may be associated with feeding the main KGV volcanoes. The thin dashed lines indicate possible lineaments identified in this study.

The main volcano of the group, Klyuchevskoy, is the tallest active volcano in Eurasia with an altitude of 4688 m, which produces moderate but frequent eruptions approximately every 3–5 years [e.g., *Khrenov et al.*, 1991; *Ozerov et al.*, 2007]. During these eruptions, high-Al and high-Mg basaltic lavas flow from the summit crater or from some of the ~80 peripheral cones of the volcano [e.g., *Khrenov et al.*, 1989, 1991].

The Bezymianny volcano, located only 10 km from Klyuchevskoy, has lavas with dacitic-andesitic composition and produces strong, explosive eruptions [e.g., *Bogoyavlenskaya et al.*, 1991; *Braitseva et al.*, 1991; *Girina*, 2013]. In 1956, after a long period of quiescence, a violent explosion that is considered one of the most important volcanic events of the twentieth century worldwide occurred on Bezymianny [e.g., *Gorshkov*, 1959; *Girina*, 2013]. Since that time, eruptions of Bezymianny have occurred roughly annually as moderate explosions that eject ash to altitudes of several kilometers [e.g., *Girina*, 2013; *Turner et al.*, 2013; *West*, 2013].

Tolbachik, the third active volcano of the group, is a basaltic fissure volcano. During the most recent eruption of Tolbachik in 2011–2012, low-viscosity basaltic lavas emerged for almost 1 year and formed large lava flows that propagated several tens of kilometers from the fissure [e.g., *Belousov et al.*, 2015; *Churikova et al.*, 2015]. Eruptions of similar sizes occurred in 1941 and in 1975–1976 [*Fedotov*, 1984; *Churikova et al.*, 2015]. Most of these eruptions occurred from fissures located to the south of the main Tolbachik summits along a large area called the Tolbachinsky Dol (Figure 1). Several historical eruptions occurred in the summit area of Plosky Tolbachik, such as in 1939 and in 1975 [*Fedotov*, 1984].

These three volcanoes, as well as numerous fresh monogenetic cones [*Churikova et al.*, 2015], seem to be associated with one lineament that propagates throughout the KGV (Figure 1), which may represent a fault zone that is completely hidden by recent volcanic deposits. In a previous tomography study of the Bezymianny and Klyuchevskoy volcanoes, *Ivanov et al.* [2016] detected alternating structures in the upper crust that correspond to the opposite flanks of this lineament and proposed that these structures may indicate lateral displacement along the lineament, which represents a strike-slip fault. The same lineament was previously identified by *Ermakov and Vazheevskaya* [1973] and *Melekestsev et al.* [1991], but it was then interpreted as a rift-associated structure.

Apart from this lineament, at the northwestern margin of the KGV, there is a large volcanic massif with a volume that exceeds the total volume of all other volcanoes of the group. It is composed of two merged volcanoes: the flat-topped Ushkovsky volcano, which reaches 3943 m in elevation, and the dormant Krestovsky volcano with an elevation of 4108 m. In addition, several cinder cones are located on the southwest and northeast flanks of Ushkovsky and form another lineament indicated in Figure 1. This structure, which appears to be nearly parallel to the Tolbachik-Bezymianny-Kluchevskoy lineament, was previously identified by *Ermakov and Vazheevskaya* [1973] and *Melekestsev et al.* [1991]. The Ushkovsky volcano formed approximately 50–60 thousand years ago. It was initially formed as a large shield volcano but subsequently grew into a large stratovolcano [e.g., *Flerov and Ovsyannikov*, 1991]. This volcano is now capped by an ice-filled 4.5 × 5.5 km caldera with two large cinder cones inside. One of these cones erupted in 1890. Present volcanic activity is evidenced by fumarole gas emission and moderate seismic activity.

In the other direction, in the southeast of the KGV, the Bolshaya and Malaya Udina volcanoes, as well as a series of cones, seem to be aligned with the Ostry and Plosky Tolbachik volcanoes. A similar lineation is observed in the Zimina massif, which is composed of several presently inactive merged volcanic edifices. All of these volcanoes may be associated with two or three northwest-oriented faults (blue dotted lines in Figure 1), which are nearly orthogonal to the line connecting the main active volcanoes of the KGV (yellow dotted line). These northwest-oriented structures may be associated with the regional-scale Kronotsk-Tigilsk fracture zone, which has been active since the Cretaceous period [*Shapiro et al.*, 1987].

In addition to the lineaments reported in previous studies, we present an interpretation for the distributions of the main volcanic cones in the KGV and other features revealed in the topographic map (Figure 1). Based on the shapes of these features, we complemented the previously proposed major lineaments with secondary lines indicated in Figure 1 with thin black dashed lines. In some areas, these lines form rather dispersed systems that cannot be approximated by a single lineament.

Based on petrological and geophysical studies [e.g., *Dobretsov et al.*, 2012], the complex eruption behavior of volcanoes in the KGV is controlled by a multilevel plumbing system. However, some of the specific mechanisms of this system remain unclear. Seismic studies are key elements to understanding the details of the

complex plumbing system of this group of volcanoes. The deep structure beneath the KGV has been investigated on different scales over recent decades in a number of geophysical studies. The shape of the slab beneath Kamchatka, which is the original cause of the arc volcanism, has been studied in a series of global [*Bijwaard et al.*, 1998; *Fukao and Obayashi*, 2013; *Grand*, 2002; *Zhao*, 2004] and regional [*Gorbatov et al.*, 2001; *Jiang et al.*, 2009; *Koulakov et al.*, 2011a] studies. Most of these studies have shown that where the Kuril-Kamchatka and Aleutian arcs meet, there is a clear gap in the subducting Pacific Plate. The KGV is located close to the edge of the slab, and this proximity may explain the exceptional intensity of volcanism in this area, as inferred from geochemical [*Yogodzinski et al.*, 2001] and seismological data [*Park et al.*, 2002]. The seismic structure of the mantle wedge above the subducting slab in Kamchatka has been studied based on data from the regional seismic network deployed by the Kamchatkan Branch of the Geophysical Survey of the Russian Academy of Sciences (KBGS) [e.g., *Gorbatov et al.*, 1997, 1999; *Nizkous et al.*, 2006; *Lees et al.*, 2007a]. A recent seismic model constructed by *Koulakov et al*. [2016a] for an area that includes the KGV and the Kizimen volcano reveals several inclined, low-velocity anomalies connecting the subducting slab with the volcanoes of this group, which suggests that the existence of several feeding paths in the mantle wedge may explain the diversity of compositions and eruption styles.

Investigation of the KGV at the crustal scale is possible because of the existence of a permanent seismic network, with as many as 25 instruments in some years, that has collected data on local seismicity for decades. Several tomographic studies of the crustal structure beneath the Klyuchevskoy volcano have been performed based on these data [e.g., *Slavina et al.*, 2001; *Khubunaya et al.*, 2007; *Lees et al.*, 2007b; *Koulakov et al.*, 2011b, 2013]. The present study is a logical continuation of previous work by *Koulakov et al.* [2011b, 2013], who followed methods similar to those used in this study. Previous seismic tomography results revealed a large anomaly of high *Vp/Vs* ratios, exceeding 2, at depths of 25–30 km beneath the Klyuchevskoy volcano [*Koulakov et al.*, 2011b]. This anomaly, which corresponds to higher *P* and lower *S* wave velocities and coincides with strong seismic activity, was interpreted as the major magma reservoir located at the crust-mantle boundary. In the middle and upper crusts, two levels of anomalies were detected, which were interpreted as intermediate and shallow magma sources. Repeated tomographic analysis has identified considerable variations of the crustal anomalies associated with eruption activity of the Klyuchevskoy and Bezymianny volcanoes [*Koulakov et al.*, 2013]. However, the anomaly associated with the deep reservoir remained unchanged. Note that the previous tomographic models were constructed based only on data from the permanent seismic network, the stations of which are sparse and unevenly distributed. Sufficient data coverage was achieved only for the local area around the Klyuchevskoy volcano; other volcanoes of the group were only slightly illuminated.

Data coverage was improved somewhat with the deployment of a temporary PIRE network on the Bezymianny volcano. This network consisted of six stations that closed some of the gaps between permanent stations [*Thelen et al.*, 2010; *West*, 2013]. Data from this network made it possible to enhance the resolution of the tomographic model of the upper crust [*Ivanov et al.*, 2016] and to demonstrate the independence of the shallow magma sources beneath the Klyuchevskoy and Bezymianny volcanoes.

There were only three permanent stations in the area of the Tolbachik volcano, which were insufficient to retrieve information about 3-D heterogeneities. To improve data coverage in and around the Tolbachik area, we initiated a field campaign to deploy a new temporary seismic network. In 1 year of recording, this network provided high-quality data that have considerably enhanced tomographic resolution throughout the KGV, especially in the south. We combined the newly derived data with picks provided by the permanent network and the PIRE network and constructed a new seismic model for the entire KGV. These new results provide important information to decipher the structure of the plumbing system that feeds the volcanoes in this group.

2. Data and Algorithms

In August 2014, we installed 24 temporary stations to supplement the 17 permanent stations operating in the KGV. Twenty of these stations consisted of Baikal ACN-87 data loggers and CME-4111 sensors, both manufactured in Russia, with recording periods of up to 30 s. The stations were powered by high-capacity chemical batteries with total volumes of 700 A h and tension of 14 volts, which was enough to feed each station for 1 year. Most of the stations were installed in areas inaccessible for land transport; therefore, the instruments were delivered by a small Robinson helicopter. Unfortunately, four stations in the northeastern part of the

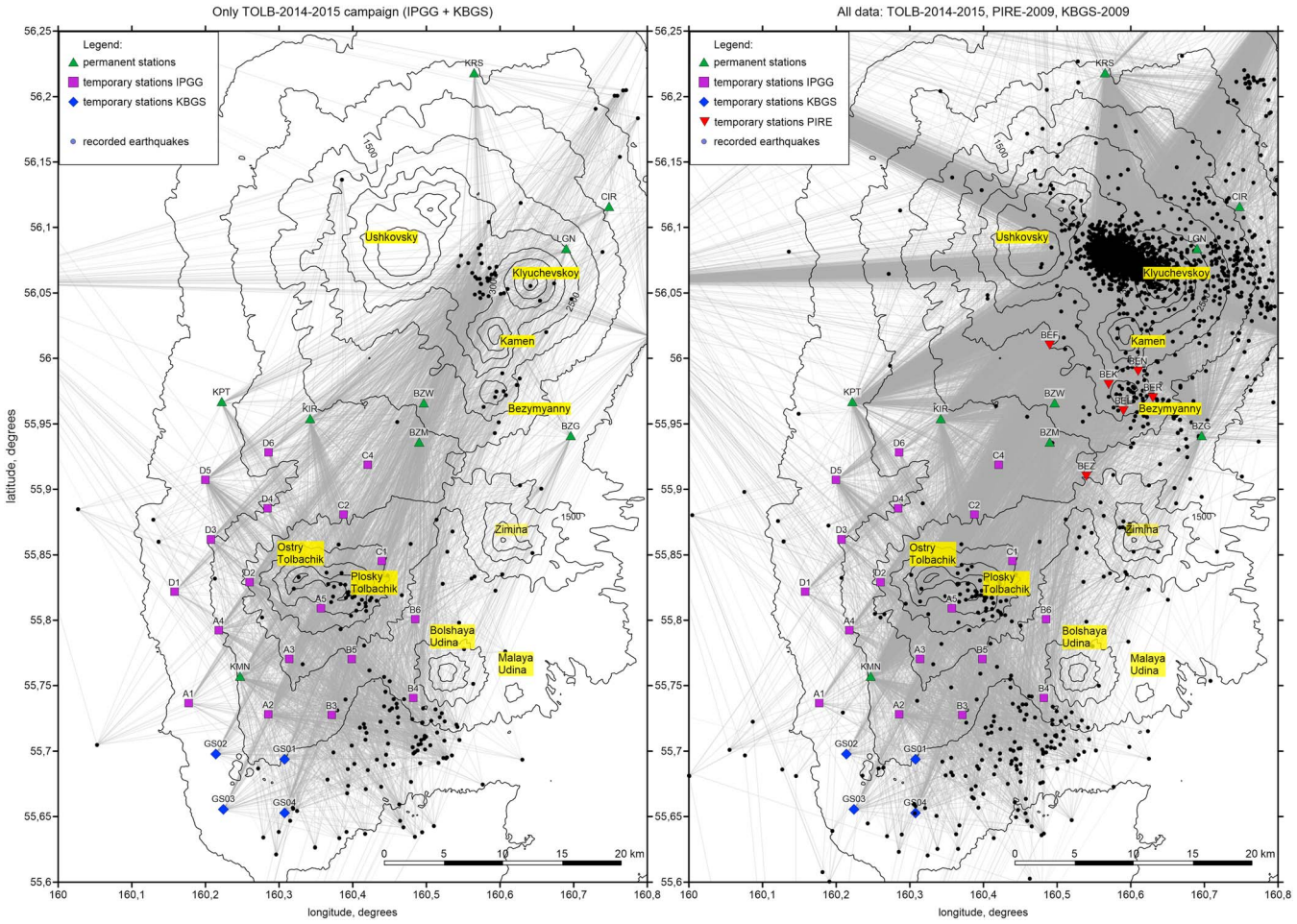

Figure 2. Data configurations corresponding to the (left) Tolbachik 2014–2015 campaign and the (right) entire data set used for tomography. The different symbols indicate stations corresponding to different networks. The black dots denote earthquake epicenters, and the gray lines are the paths of *P* wave rays. The topography is represented by contour lines with intervals of 500 m. The yellow captions indicate volcano names.

network were destroyed by bears. For two of these stations, the data were completely lost. During the first 3 months of operation, the network was supplemented by four additional Guralp broadband stations deployed by the KBGS in the southern part of the Tolbachinsky Dol. The network operated autonomously for 1 year and was terminated in the summer of 2015. At the beginning, 22 temporary stations operated simultaneously (Figure 2); the number of live stations then gradually decreased to nine for several reasons, such as bear attacks, flooding, and freezing of batteries and instruments.

When processing the data and picking the arrival times of seismic waves, we mainly used event identifications provided by the KBGS monitoring survey. Among these, we selected the events that provided the most optimal ray coverage to perform tomographic inversion (Figure 2a). For example, several thousand events occurred in the KGV during the studied period in one deep cluster just beneath the Klyuchevskoy volcano (Figure 2b). For the Tolbachik network, these events were located outside the network area, and measuring a large number of picks from these events would not be useful because the corresponding rays form similar paths. Therefore, we selected only the 20 clearest events from this cluster and aimed to select as many events as possible from other parts of the KGV to achieve the most homogeneous ray coverage possible. In total, for the temporary network in Tolbachik supplemented with permanent stations operated in the same period, we have selected 230 local events that occurred in the KGV during the observation period and manually picked the arrival times of 3698 *P* and 3964 *S* waves, which enabled ~33 picks per event. For picking, we used the DIMASS software [*Droznin and Droznina*, 2011], which is the main tool used for seismic processing by the KBGS. Two examples of data picking of preliminary source locations, one for a strong event at ~25 km

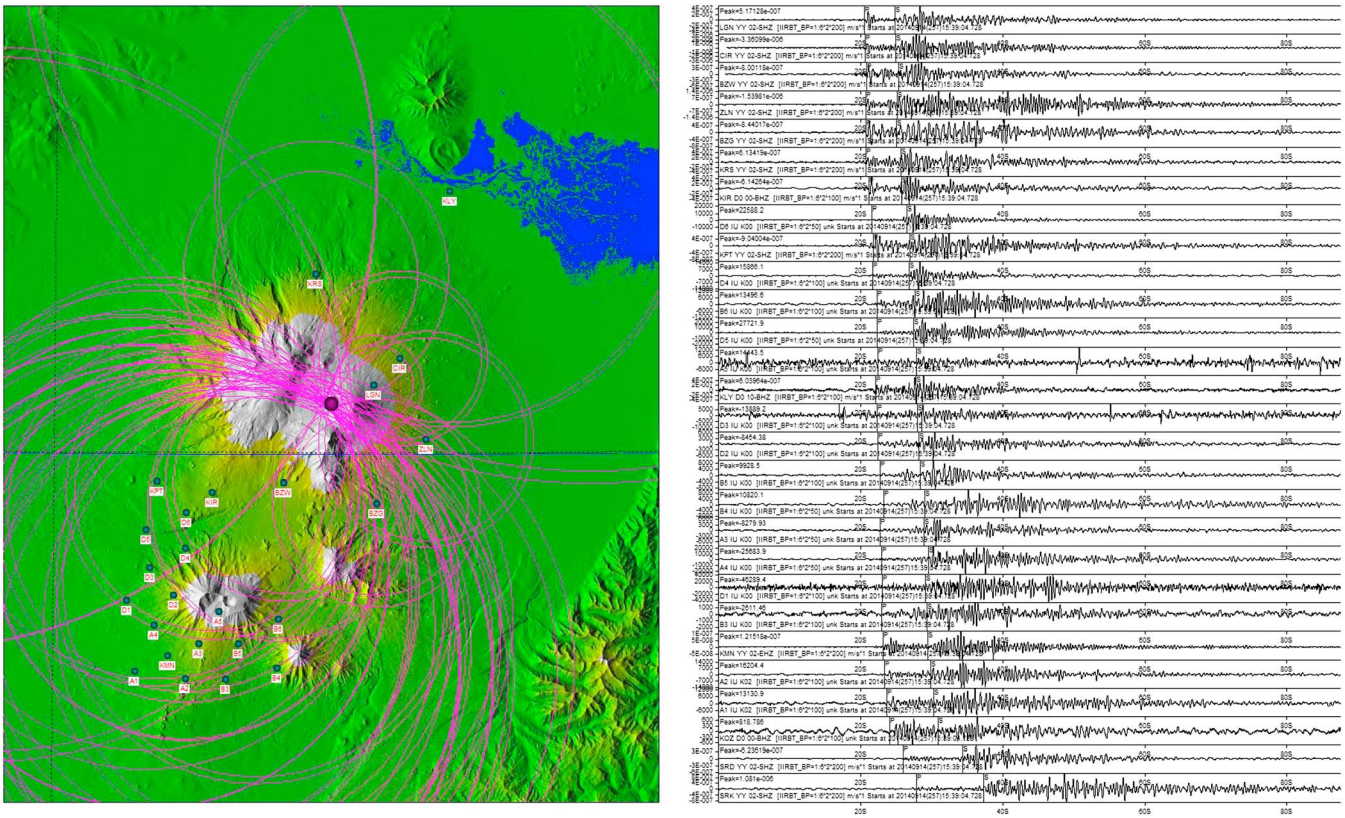

Figure 3. Examples of data processing using the DIMASS software with the preliminary location of the events and a picking monitor. Two cases are represented: (a) a strong event beneath the Klyuchevskoy volcano and (b) a weaker event located south of Tolbachik.

depth beneath the Klyuchevskoy volcano and another for a weaker event at ~15 km depth south of Tolbachik, are presented in Figure 3.

In addition, we have used data from the temporary PIRE network installed on Bezymianny in October–December 2009 [*West*, 2013; *Ivanov et al.*, 2016]; this data set included the arrival times of 2256 *P* waves and 1951 *S* waves from 333 events (12.6 picks per events). This data set was previously used for studying the seismic structure of the upper crust beneath the Bezymianny volcano [*Ivanov et al.*, 2016]. Finally, we used the entire catalogue of the KBGS for the same observational period, which included more than 48,000 picks for 2810 events. A summary of the ray coverage for all of the data used for tomography is presented in Figure 2b. Although the subset that corresponds to the KBGS permanent network provided the most data, the ray coverage of these data was not as good as that of data from the new Tolbachik network.

To select the experimental data for tomographic inversion, we used the following criteria. (1) The residuals after source locations in the initial 1-D velocity model should not exceed 0.8 s and 1.3 s for the *P* and *S* wave data, respectively, which are determined based on the expected sizes and intensity of anomalies in the KGV. (2) The minimum number of the *P* and *S* wave phases should be no less than 8. (3) The seismicity should be located beneath the KGV at depths of no deeper than 40 km. No slab-related seismicity was taken into consideration, because for the existing aperture of the network (at least for the temporary stations around Tolbachik), it would mostly provide vertical rays without crossing in the study volume, and therefore, such rays would hardly be useful for tomography. In total, for tomography, we selected 3196 events, 230 of which were recorded by the temporary network installed in 2014–2015, which were particularly important for providing adequate resolution for the Tolbachik area. After selection, 25,102 *P* and 30,072 *S* wave picks were used for tomography. The higher number of *S* wave data is attributed to the higher amplitude of the *S* wave signal, which is more robustly identified in cases of noisy data on active volcanoes.

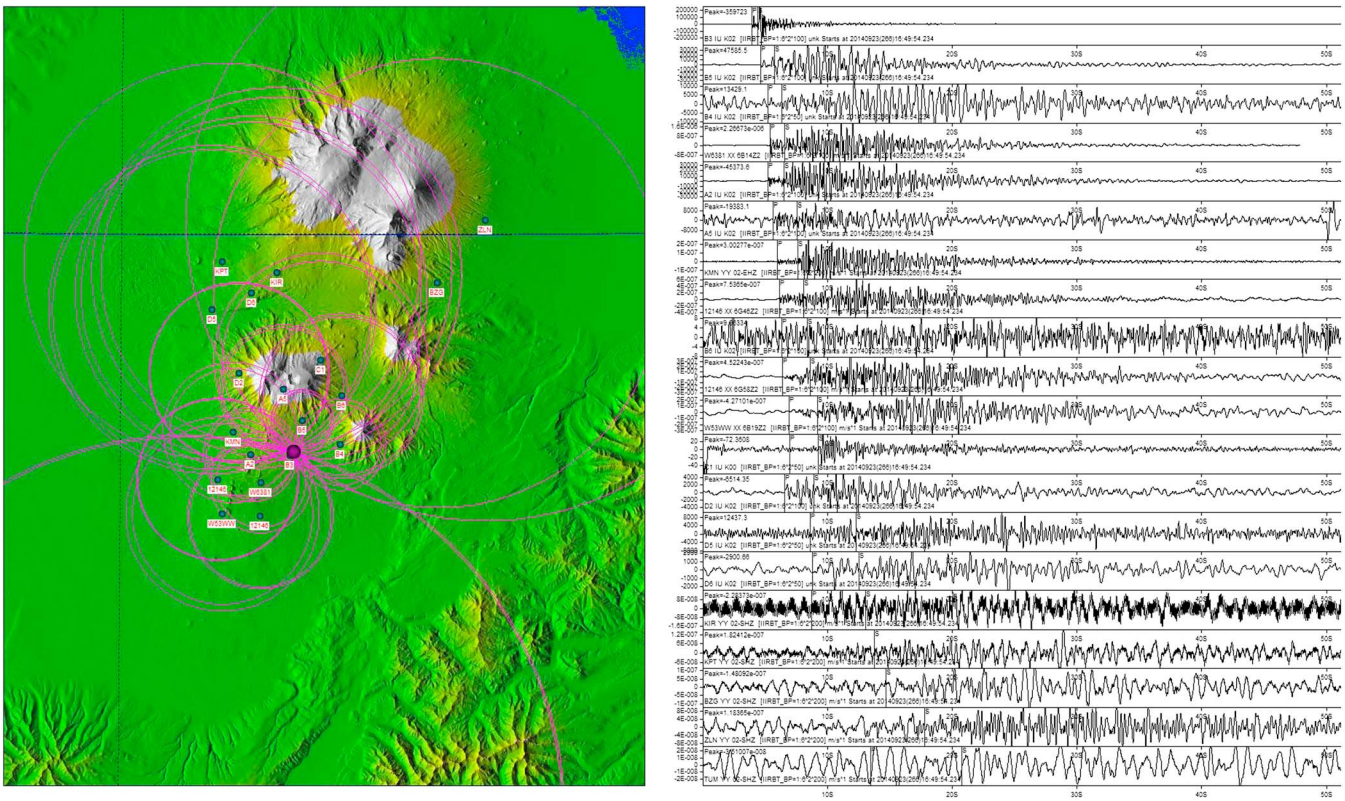

Figure 3. (continued)

The tomographic inversion was performed using the LOTOS code [*Koulakov*, 2009], which enables simultaneous inversion of the velocities of *P* and *S* waves and source parameters. This code has been described in a number of papers and in the user manual, which is available with the open-access version of the code at www.ivan-art.com/science/LOTOS. Therefore, we only briefly summarize the major steps of this procedure.

The workflow begins with the preliminary location of sources using a multigrid search method. The search starts from a grid with a large node spacing. If the best solution is achieved in a node located at the border of the grid, the search is repeated for another grid centered in this node. After finding a node with the absolute extremum of the goal function, the search continues using finer grids. This location algorithm is not dependent upon the starting point of the sources and provides robust solutions even if the starting point for the source search is located very far from the true location. At this step, many initial locations based on the data from the permanent network the KBGS were shifted considerably when data from the temporary stations were added.

At this step, we optimized the initial reference model using the grid search method for the velocity and *Vp/Vs* ratio. The initial model for the *P* wave velocity was defined at several depths with linear interpolation between them. The *S* wave velocity was set based on a constant *Vp/Vs* ratio. When optimizing the model, we changed the *Vp/Vs* ratio from 1.4 to 1.85 with an increment of 0.02 and changed the *P* wave velocity to a constant deviation for all depths in the range of −1 to 1.5 with an increment of 0.2. For each velocity model, we performed source location and computed the residual deviations in the *L1* norm. The results of the grid search for two different initial *P* wave velocity models are shown in Figure 4. The minimum value of the residual norm at these plots represents the best solution for the velocity model. We have evaluated several different starting models, but here we present only two cases with considerably different starting gradients in the *P* wave velocity model. Despite the differences between the gradients in the *P* wave velocity models, the *Vp/Vs* ratio for the best models remains stable at a value of 1.7. The final 1-D reference model that

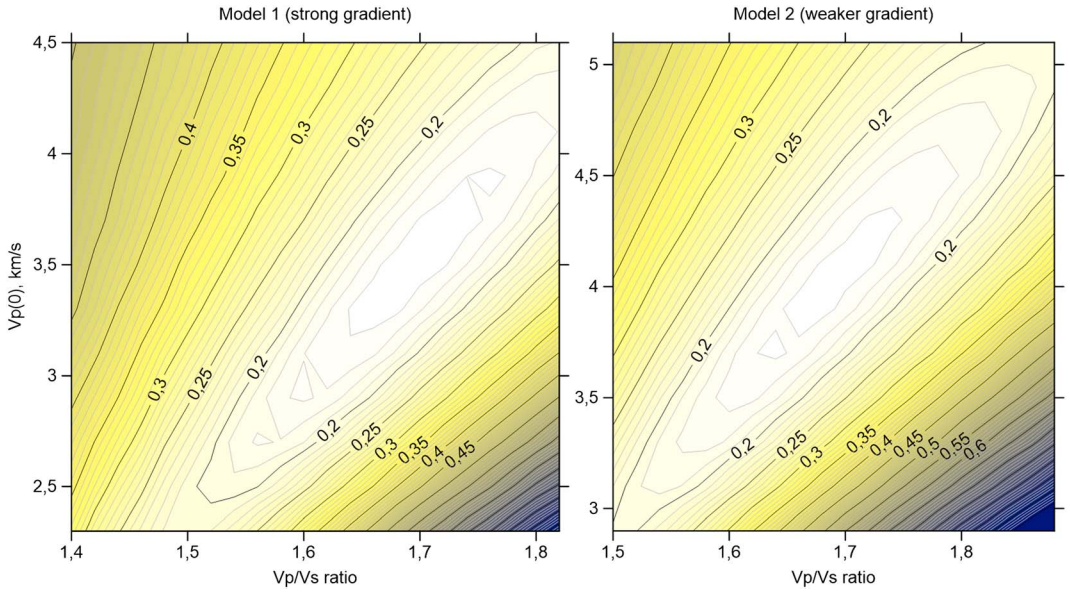

Figure 4. Average residuals computed in the L1 norm used for the grid search of optimal *P* wave velocities and *Vp/Vs* ratios. The two plots present examples of results for two different starting velocity models with stronger and weaker gradients.

provides the best data fit is presented in Table 1. Between the indicated depth levels, velocity was linearly interpolated. No velocity jump on the Moho was predefined in this model.

The following analysis was performed according to the standard LOTOS procedure. The iteration begins with another location step, in which travel times are computed using a 3-D ray tracing based on the bending method, whose basic principle was proposed by *Um and Thurber* [1987]. The velocity distribution is parameterized by nodes installed according to the ray density. To minimize the effect of grid geometry, inversions are performed for several grids with different basic orientations of the nodes; the inversion results are then averaged and recomputed in a uniform grid. This model is used for the input velocity distribution for source location in the next iteration. The simultaneous matrix inversion for the *P* and *S* wave velocity parameters and source corrections is performed using the Least Squares with QR factorization algorithm [*Paige and Saunders*, 1982; *Nolet*, 1987]. The matrix also includes special components that control the amplitudes and flattening of anomalies.

3. Synthetic Modeling and Experimental Data Inversion

Before discussing the main seismic model derived after inversion of the experimental data, we present several synthetic tests. In addition to helping to assess the spatial resolution, synthetic modeling may help us determine the optimal values of free inversion parameters to enable the best possible recovery quality.

Synthetic modeling is performed to simulate the workflow of experimental data processing as closely as possible. Synthetic travel times are computed using 3-D ray tracing through the predefined synthetic model. The data are perturbed with noise to enable the same variance reduction as in the case of experimental data inversion. Any information about the sources and velocity model is then "forgotten," and the recovery procedure begins with the absolute locations of sources in the initial 1-D model.

Table 1. *P* and *S* Wave Velocity Distributions in the 1-D Reference Model Used for Inversion

Depth, km	*Vp*, km/s	*Vs*, km/s
−5	4.16	2.33
0	4.24	2.37
10	5.10	3.03
20	5.94	3.48
30	6.76	3.91
55	8.10	4.79
300	8.40	4.94

Here we consider three different types of synthetic test. The first model is a regular checkerboard with alternating positive and negative

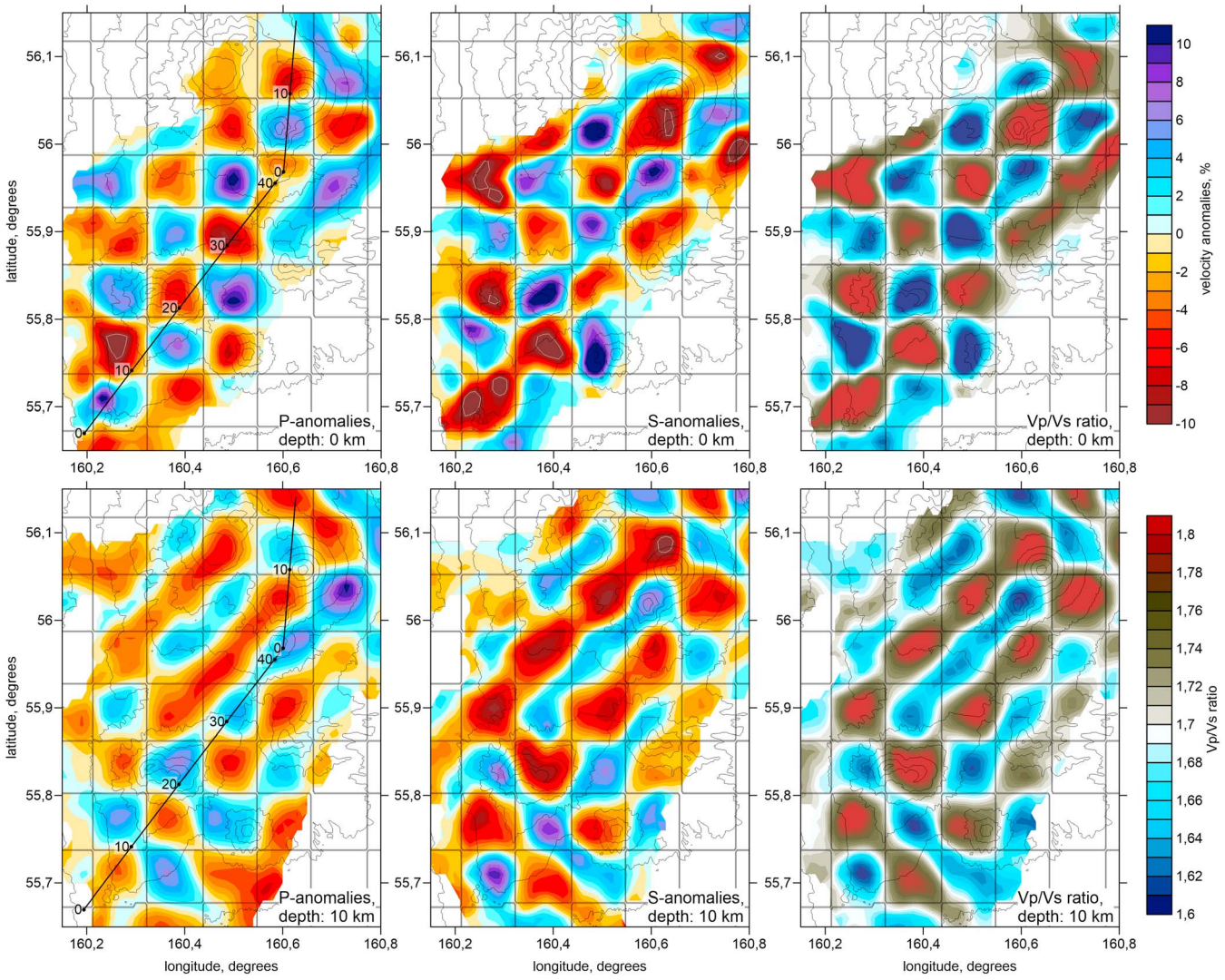

Figure 5. Recovery results for the *P* and *S* wave anomalies and the *Vp/Vs* ratio for the checkerboard model with the transition of the anomaly sign at 5 km depth. The configuration of the synthetic anomalies is highlighted with lines. Topography is represented by contour lines with intervals of 500 m.

anomalies with sizes of 7 km and amplitudes of ±5% and ±7% for the *P* and *S* wave anomalies, respectively. We defined the opposite signs for the *P* and *S* wave anomalies to simulate strong variations of the *Vp/Vs* ratio. With depth, the anomaly sign changes first at a depth of 5 km and then again every 15 km. The recovery results at depths of 0 and 10 km, which correspond to the first and the second layers of anomalies, are shown in Figure 5. The shapes of anomalies in both layers with opposite sign values are correctly recovered for both *P* and *S* wave anomalies and, especially, for the *Vp/Vs* ratio. The results of this test demonstrate fair vertical resolution for the upper crustal structures throughout the entire study area. A particularly high resolution is achieved in the area of the Tolbachik volcano, where numerous, regularly distributed seismic stations were installed.

In the second series of tests, we focused on the vertical resolution along several selected profiles. Along profiles 1 and 2, which pass through the Tolbachik, Bezymianny, and Klyuchevskoy volcanoes, we defined a model with checkerboard anomalies (Figure 6) 7 × 6 km in size in the horizontal and vertical directions, respectively, so that the anomaly sign changed every 6 km in depth, e.g., at 3, 9, 15, and 21 km. Across this section, the anomalies remain unchanged within a 10 km thick layer. As in the previous test, the amplitudes of anomalies were ±5% and ±7% for the *P* wave and *S* wave anomalies, respectively, and these anomalies had opposite signs. The inversion results show fair recovery of sign transitions at the depths of 3 km and 9 km and

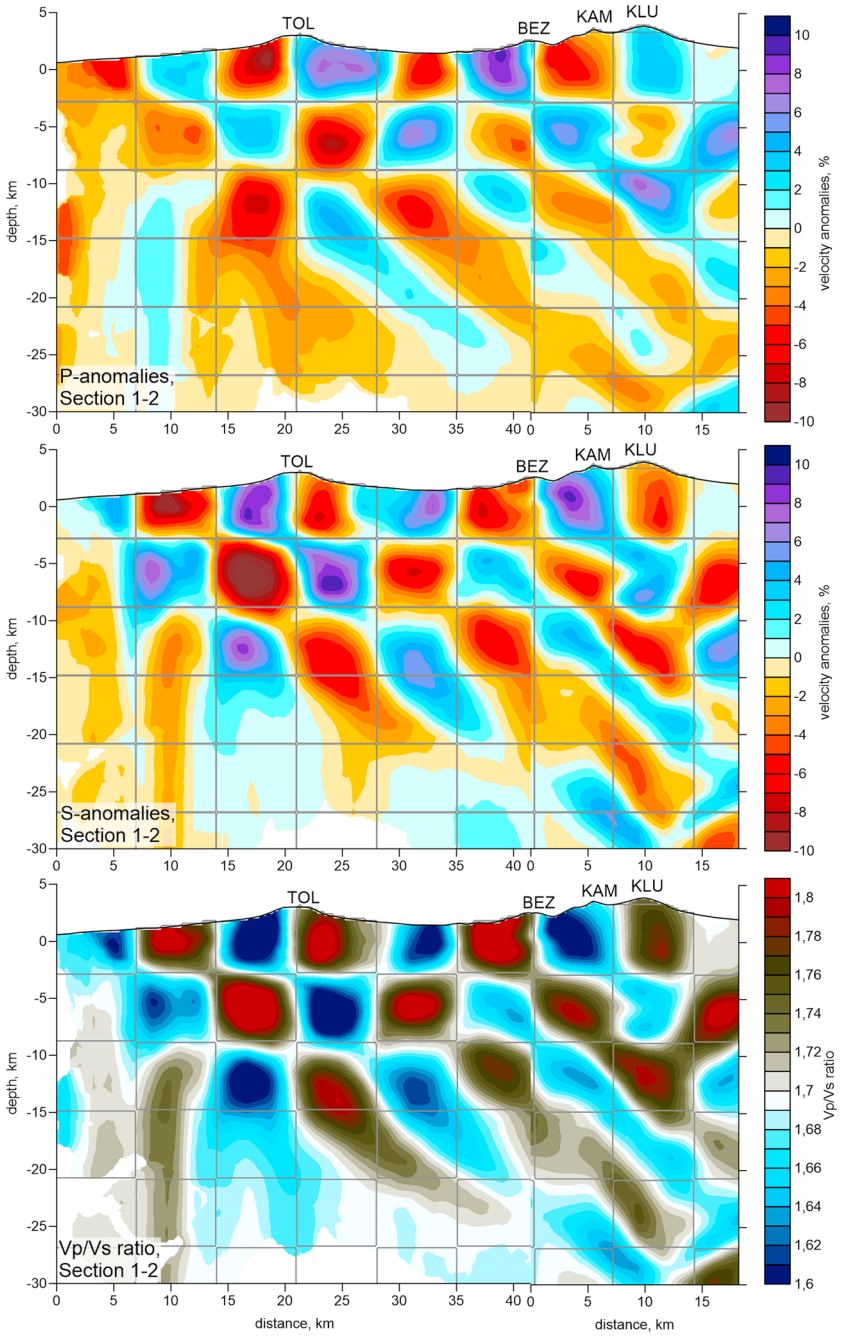

Figure 6. Recovery results for the *P* and *S* wave anomalies and the *Vp/Vs* ratios for the checkerboard model defined in sections 1 and 2 (see location in Figure 5). The configuration of the synthetic anomalies is highlighted with lines. Abbreviations are volcano names: TOL: Tolbachik, BEZ: Bezymianny, KAM: Kamen, KLU: Klyuchevskoy.

correct reconstruction of anomalies in the upper three layers for the entire profile. The deeper structures can only be recovered for the part of the section that corresponds to the Klyuchevskoy volcano where most of the deep seismicity is located.

The actual resolution of realistic structures was checked using another synthetic test presented in Figure 7. For the same profile considered in the previous test, we have defined the model with polygonal definitions of anomalies that have similar shapes to those derived from inversion of experimental data. We defined the values of the *P* and *S* wave anomalies that yield high and low *Vp/Vs* ratios similar to those observed in the main results. In Figure 7, we present the recovering results for *Vp/Vs* ratios only. For the upper crust, all

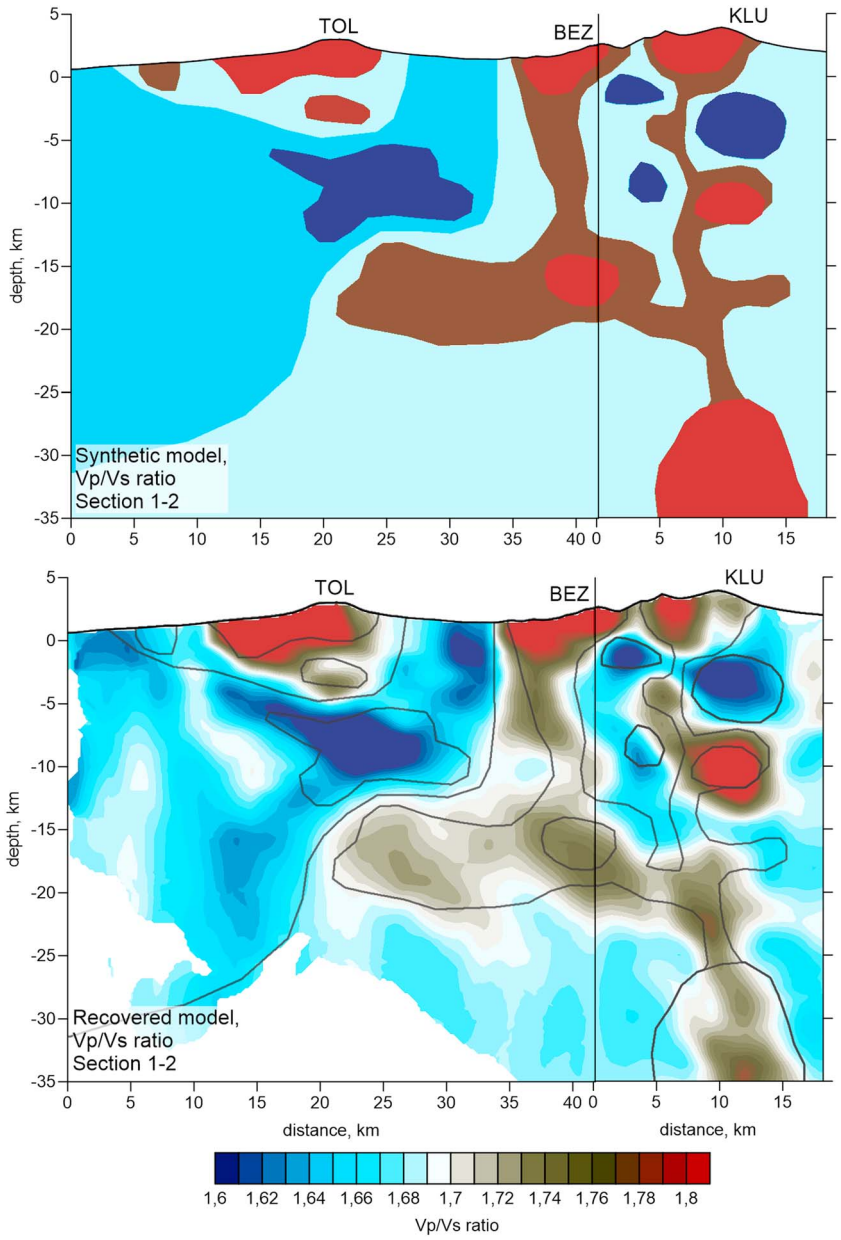

Figure 7. Recovery results for *Vp/Vs* ratios of the checkerboard model defined in sections 1 and 2 (see location in Figure 8). The configuration of synthetic anomalies is highlighted with lines. Abbreviations are volcano names: TOL: Tolbachik, BEZ: Bezymianny, KAM: Kamen, KLU: Klyuchevskoy.

structures along the profile are resolved correctly. Starting from the depth of 10 km, only the shapes of anomalies can be recovered, but their magnitudes are reduced compared with the original synthetic model. This finding should be taken into account when interpreting the experimental data results; the actual values of anomalies may appear stronger than those derived in the computed model.

To invert the experimental data, we used five iterations of the tomography workflow. Table 2 presents the values of average residual deviations computed in the L1 norm and variance reduction obtained during the iterative inversion of experimental data. These results show that we have obtained moderate values of variance reduction of 23.5% and 27% for the *P* and *S* wave data, respectively, which are typical values for volcano tomography studies. These values are mostly related to high levels of natural noise and scattering of seismic waves that may decrease the accuracy of *P* and *S* wave picking. The final values of the residuals

Table 2. Deviations of the *P* and *S* Wave Residuals (in the L1 Norm) and Their Reduction During the Inversion of Experimental Data

Iteration	*P* Residual Deviation, s	*P* Residual Reduction, %	*S* Residual Deviation, s	*S* Residual Reduction, %
1	0.180	0	0.242	0
2	0.148	17.7	0.192	20.8
3	0.142	21.0	0.183	24.5
4	0.139	22.6	0.179	26.0
5	0.138	23.5	0.177	27.0

(0.138 s and 0.177 s for the *P* and *S* wave data, respectively) are of the same order of magnitude as the estimated accuracy for arrival time picking.

Through inversion, we have obtained the locations of seismic events identified in the final 3-D velocity model. The new seismic network has provided the accurate locations of events in the Tolbachik area for the first time. Previously, such events were localized by very sparse stations that could not provide any robust solution. With this new data, we have identified groups of earthquakes that elucidate processes in the plumbing system beneath the volcano, as discussed in the next section.

The distributions of anomalies of *P* and *S* wave velocities and *Vp/Vs* ratio at depths of 0, 8, 16, and 30 km, as well as the seismicity at the corresponding depth intervals, are presented in Figures 8–10. Furthermore, we present the distributions of the same seismic parameters in several key profiles in Figure 11. Profiles 1 and 2 start in the Tolbachinsky Dol close to the North Vent of the 1975 eruption, pass through the summit of the Plosky Tolbachik volcano to the Bezymianny volcano, and then they turn and pass through the Kamen and Klyuchevskoy volcanoes. Section 3 reveals the distributions of anomalies across Tolbachik in the SE-NW direction. The anomalies beneath the Kluchevskoy and Ushkovsky volcanoes are shown in section 4 in an NW-SE orientation. The resulting seismic velocity structures and the distributions of localized seismicity are discussed in detail in the following section.

4. Discussion

In general, for the areas of the Klyuchevskoy and Bezymianny volcanoes, we have obtained similar seismic structures to those derived in most previous studies of this. For example, similarly as in *Koulakov et al*. [2011b] and *Koulakov et al.* [2013], beneath the Klyuchevskoy volcano, we have identified three anomalies of low *Vs* and high *Vp/Vs* ratio located at around zero level and at depths of 10 km and 25–30 km. Beneath Bezymianny, we found a strong shallow anomaly of very low *Vs* and high *Vp/Vs* ratio that is generally consistent with the result by *Ivanov et al.* [2016]. At the same time, for the Tolbachik area, we have identified completely new seismic structures and accurate locations of seismic events because of the new data recorded by our temporary network in 2014–2015. In the previous studies, this area with only one permanent station was not sufficiently illuminated by seismic data; therefore, no information on seismic structure could be obtained. The new data presented here have provided new insight into the processes beneath Tolbachik and possible explanations for the causes of recent large fissure eruptions. Furthermore, the data from the new network made it possible to improve the accuracy of source locations for some events, which enabled us to draw certain conclusions related to the structures of the plumbing system beneath the Klyuchevskoy group volcanoes.

Links between shallow seismic anomalies and the main volcano-related structures and lineaments of the study area are identified in Figure 12. The main volcanic area of the Bezymianny, Kamen, and Klyuchevskoy volcanoes is associated with very strong low *S* wave velocity anomalies and high *Vp/Vs* ratios. These findings may represent fresh layers of pyroclastics and other soft volcanic rocks deposited by frequent and voluminous eruptions. Saturating such relatively soft sediments with meteoric water should result at decrease of the *S* seismic velocity and increase of *Vp/Vs* [e.g., *Han and Batzle*, 2004]. Among these volcanoes, only Kamen seems to be associated with a local increase in velocity, which may represent a remnant solid igneous body associated with this dormant volcano. A similar local feature, which may have the same cause, is observed to the south of the Klyuchevskoy volcano.

Ushkovsky, which is an immense volcanic complex with a total volume larger than all other volcanoes in this region combined [e.g., *Flerov and Ovsyannikov*, 1991], is mainly located outside the resolved area; however,

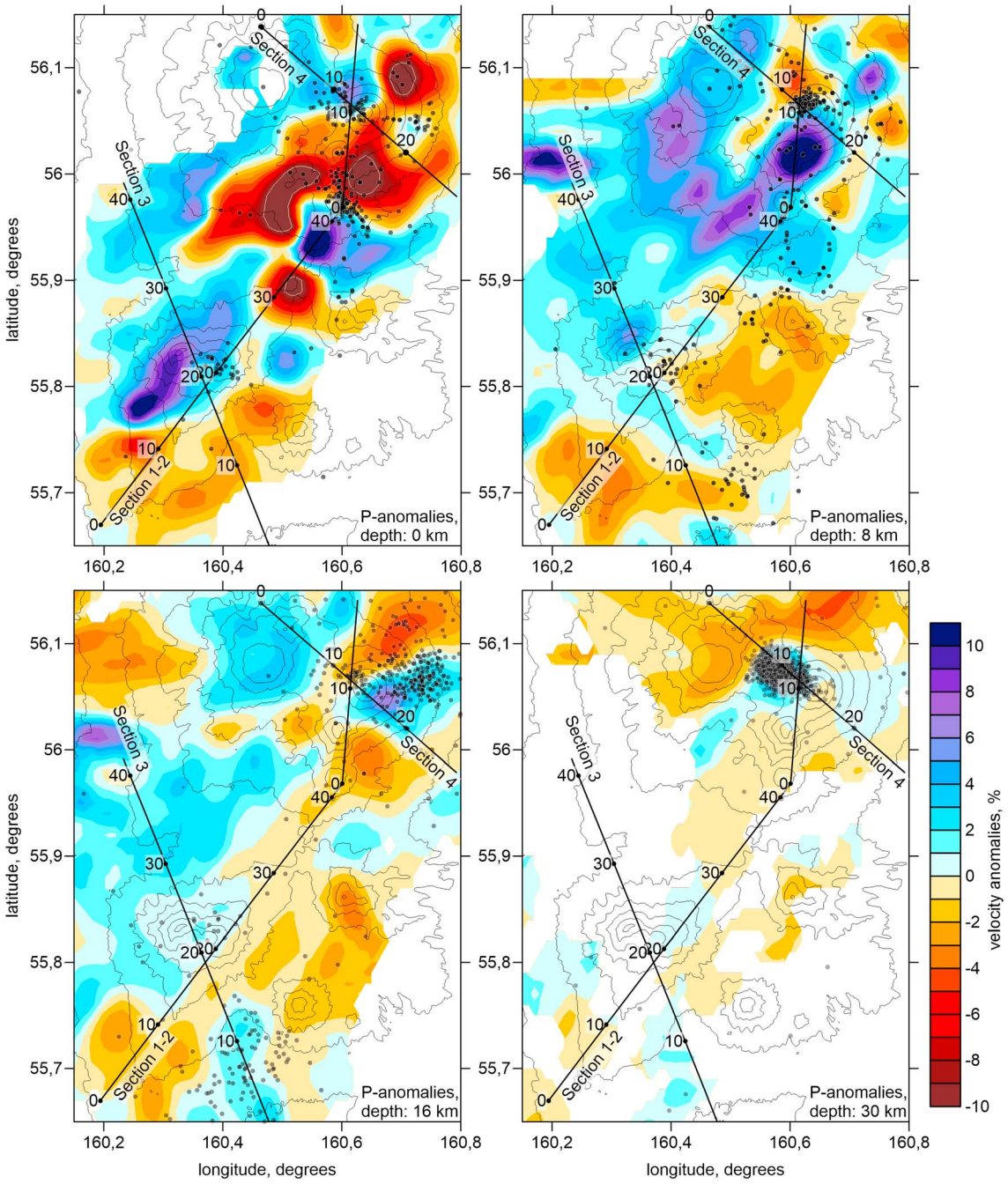

Figure 8. Resulting *P* wave velocity anomalies in horizontal sections. The relocated seismicity at the corresponding depth intervals is depicted with yellow dots. Topography is represented by contour lines with intervals of 500 m.

the general trend of velocity increase beneath this volcano is apparent. The predominantly basaltic composition of this volcano forms a large solid igneous body with relatively high seismic velocities. Similar high-velocity anomalies are observed beneath Ostry Tolbachik and partly beneath Plosky Tolbachik. These volcanoes also have basaltic compositions [e.g., *Churikova et al.*, 2015] and appear in our seismic model in a similar way as does Ushkovsky.

An interesting link can be identified between the shallow anomalies and the distribution of lineaments determined from the distributions of monogenetic cones and certain tectonic structures reflected in the topography (Figure 12). The clearest lineament is observed along two branches located at opposite sides of the Plosky Tolbachik volcano. The southwest lineament forms the Tolbachinsky Dol, an

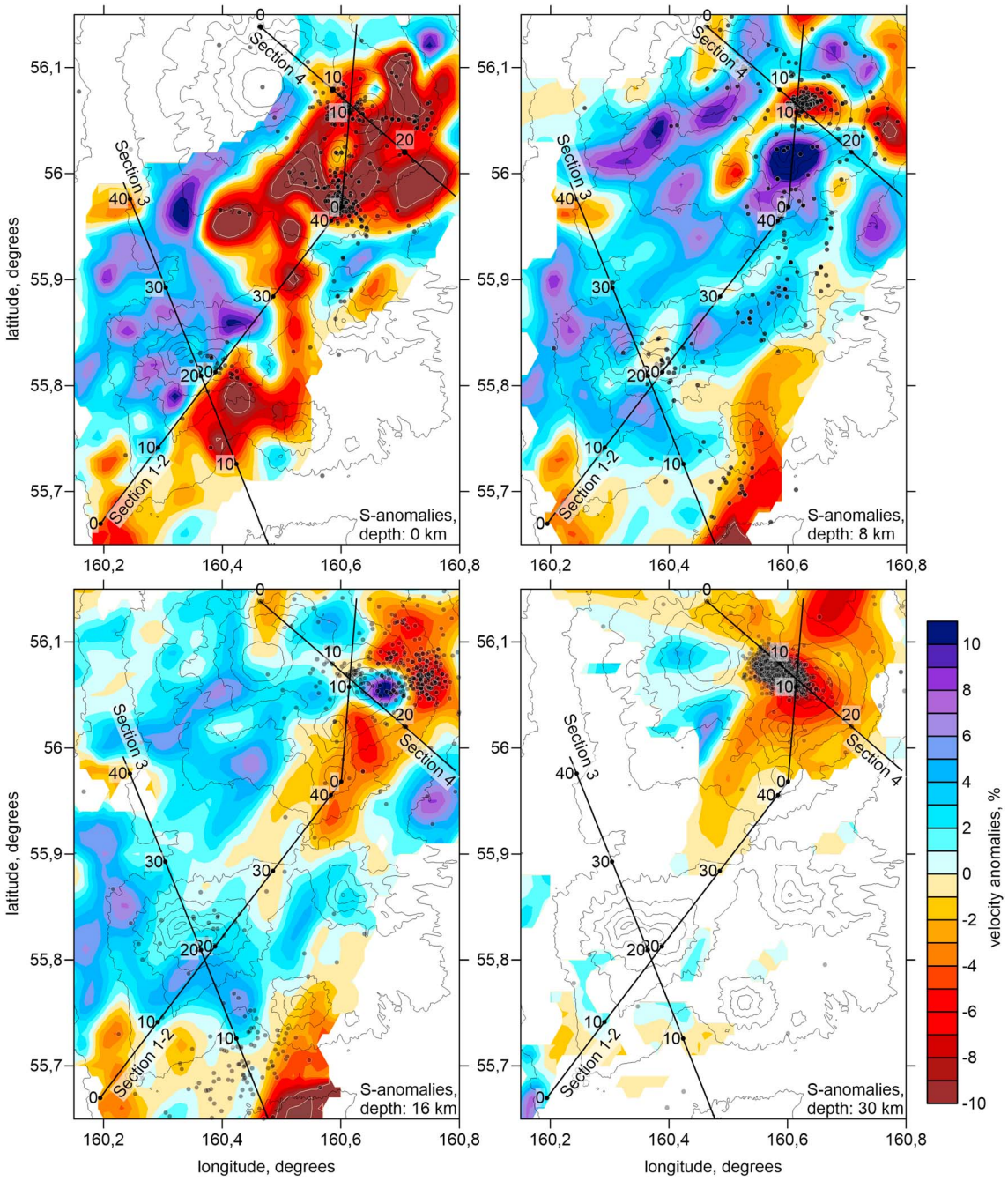

Figure 9. Same as Figure 8, but for *S* wave velocity anomalies.

area of ~40 km in length where frequent fissure eruptions have recently occurred. To the northeast, a series of well-expressed cones form another linear structure oriented toward the Bezymianny volcano. Together, these two branches form a lineament that clearly coincides with the boundary between the high- and low-velocity anomalies in the shallow section (Figure 12). We propose that this structure may be associated with the regional fault that passes throughout the KGV marked by the presently active Tolbachik, Bezymianny, and Klyuchevskoy volcanoes. The same hypothesis was also proposed by *Ivanov et al.* [2016], who found similar linear alternations in shallow seismic structures in the area of the Bezymianny volcano. Clear changes in the seismic structures on the opposite flanks of this fault zone may indicate considerable lateral displacement causing step-shaped configurations of anomalies.

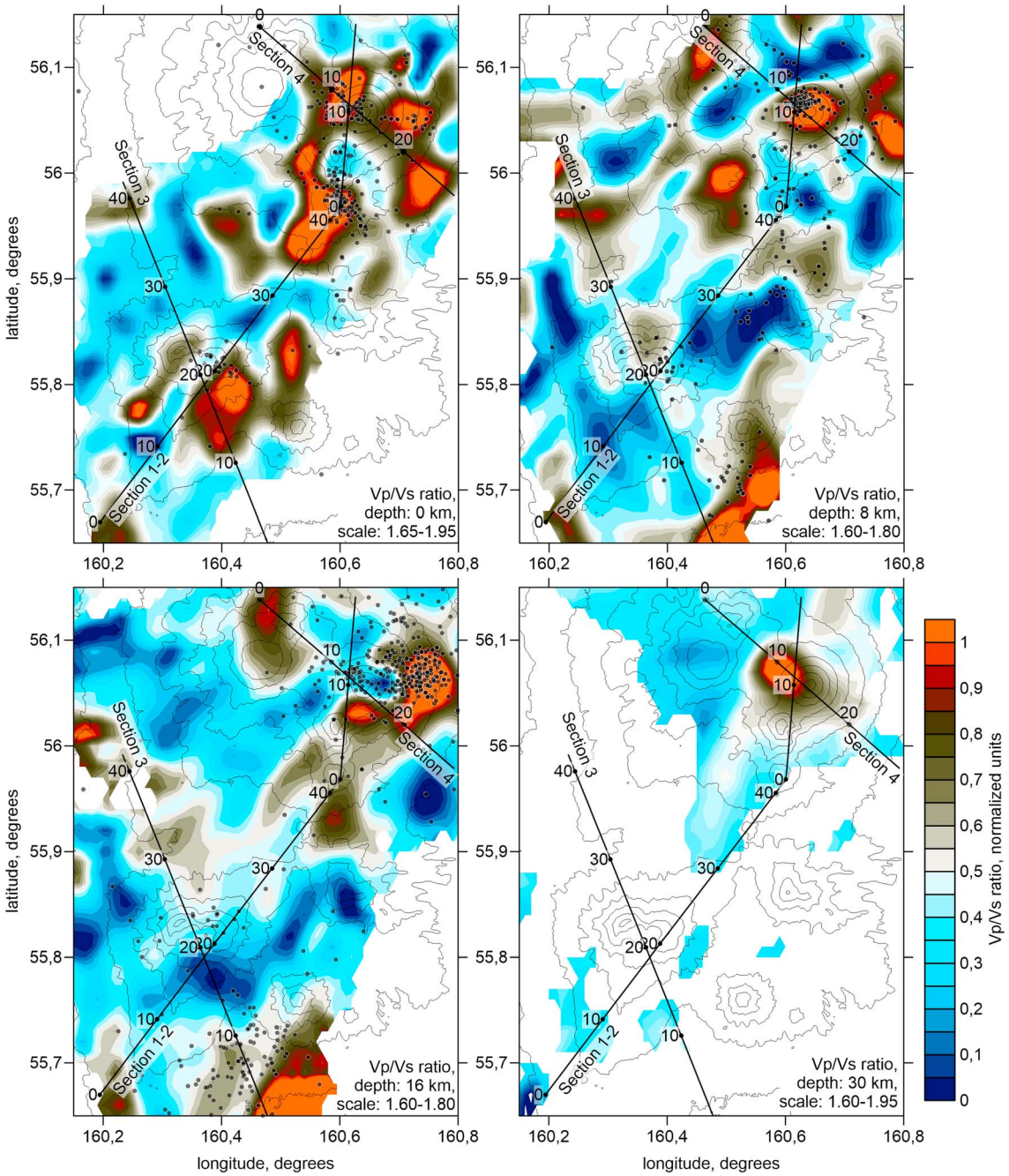

Figure 10. Same as Figure 8, but for *Vp/Vs* ratios. The range of the *Vp/Vs* ratio color scale is indicated in the legend on each plot.

Another parallel lineament, represented by a series of monogenetic cones in the western part of the KGV, seems to also be associated with the linear velocity contrast that passes through the Ushkovsky volcano. This finding may indicate a zone of another fault hosting the Ushkovsky volcano and the related cones, which presently seem to be inactive. Based on this hypothesis, we propose that the activity of the KGV has been controlled primarily by two nearly parallel strike-slip faults, one of which is presently active and hosts the Tolbachik, Bezymianny, and Klyuchevskoy volcanoes.

Beneath all of the active volcanoes, in the uppermost crust, we observe very high values of *Vp/Vs* ratios, typically exceeding 1.9 and sometimes even 2. In vertical sections, these anomalies may reach depths of 2 to 4 km. These features may represent soft deposits of volcanoclastic rocks highly saturated with fluids (e.g., meteoric water). These anomalies may also be related to shallow magma reservoirs that behave as

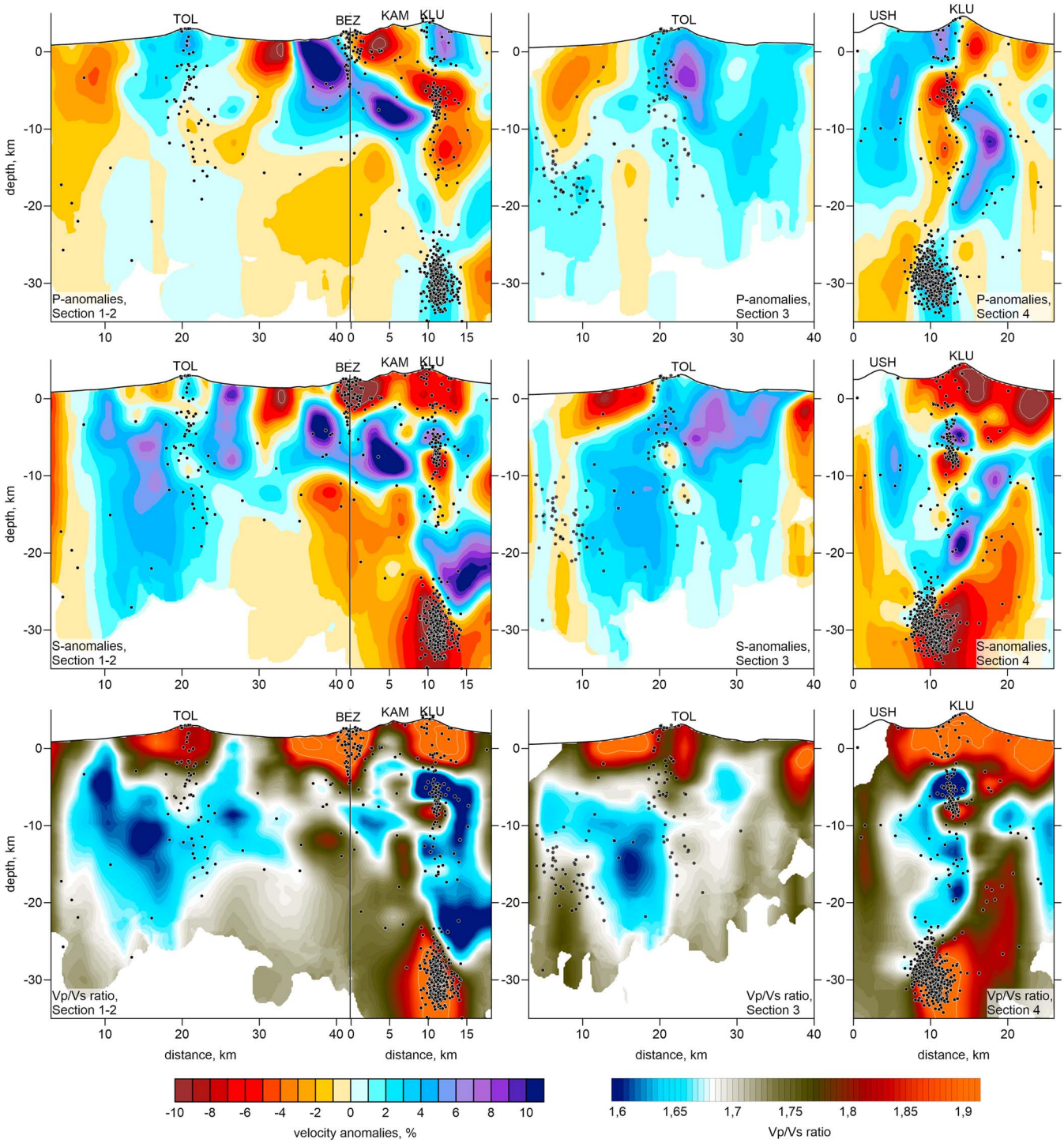

Figure 11. The resulting *P* and *S* wave velocities and *Vp/Vs* ratios in the vertical sections with locations indicated in Figures 8–10. The black dots denote earthquakes located within 3 km of the profile. The major volcanoes are indicated as follows: TOL: Tolbachik, BEZ: Bezymianny, KAM: Kamen, KLU: Klyuchevskoy, USH: Ushkovsky.

sponges highly saturated with fluids and melts [see, for example, *Han and Batzle*, 2004; *Watanabe*, 1993]. To reach more definitive conclusions about these upper crustal structures, further investigations providing higher vertical resolution, such as using the ambient noise tomography, are required.

The results of seismic tomography inversion and the relocated seismicity distributions reveal three different types of feeder regime for the Klyuchevskoy, Bezymianny, and Tolbachik volcanoes, which are schematically illustrated in Figure 13.

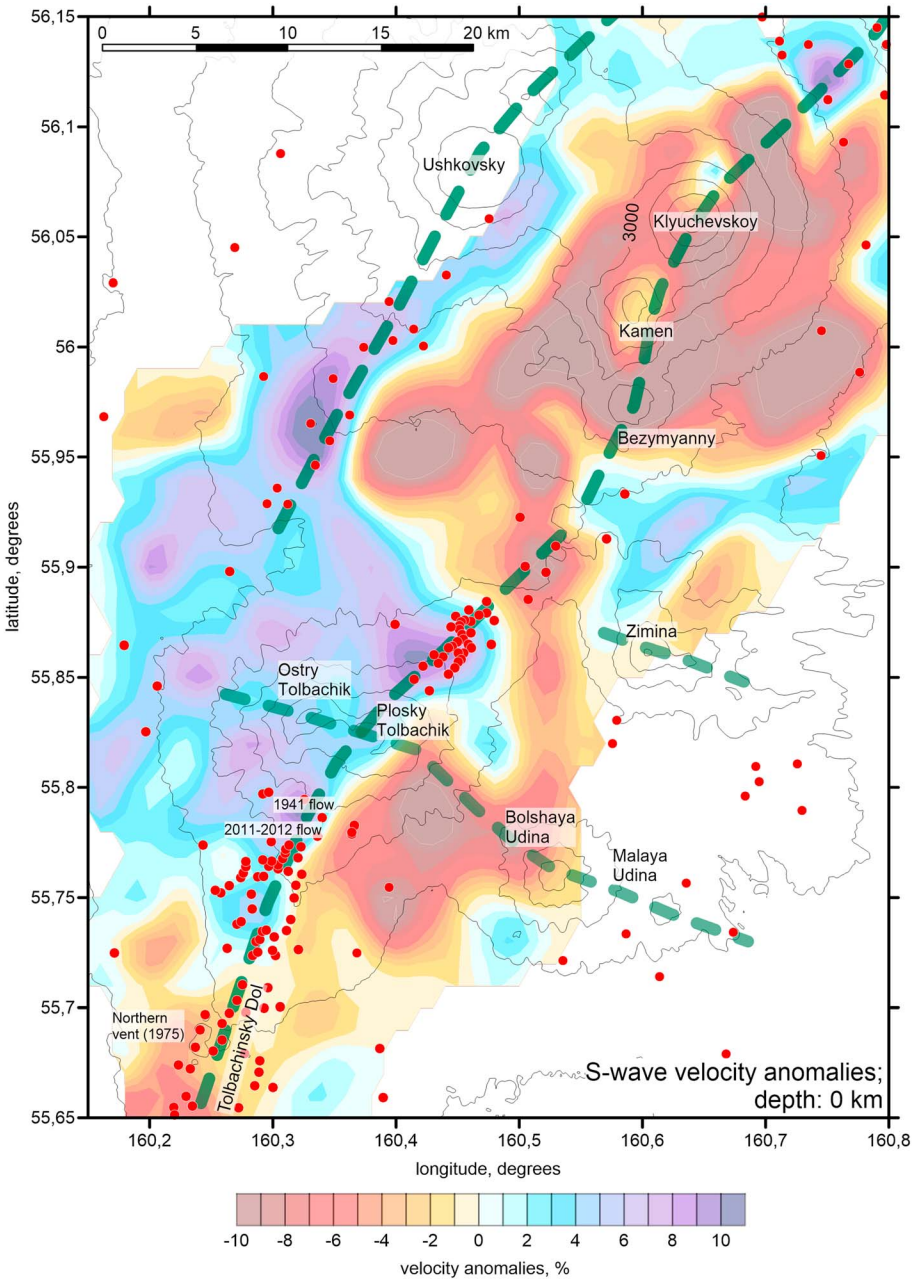

Figure 12. Comparison of the shallow structures of *S* wave velocity anomalies (depth 0 in Figure 9) with the main volcanic structures and lineaments indicated in Figure 1.

4.1. Klyuchevskoy Volcano—High-Pressure "Pipe"

Beneath the Klyuchevskoy volcano, the structures of *P* and *S* wave velocities and the *Vp/Vs* ratio appear to be very heterogeneous (Figure 14). Based on the results of the synthetic tests, we conclude that the spatial resolution is sufficient to resolve these heterogeneities. The most striking feature in this part of the model is a structure at depths below 25 km where high *P* and very low *S* wave velocity anomalies result in very high *Vp/Vs* ratios exceeding 2. A similar anomaly was observed in previous tomography studies [*Koulakov et al.*, 2011b], and this anomaly was found to remain stable in repeated tomographic inversions over 10 years [*Koulakov et al.*, 2013]. Within this anomaly, very strong seismic activity occurs continuously, as recorded during long-term instrumental observations. We propose that this feature represents the top of the mantle conduit that brings large amounts of volatiles and melts. The occurrence of strong seismicity around the

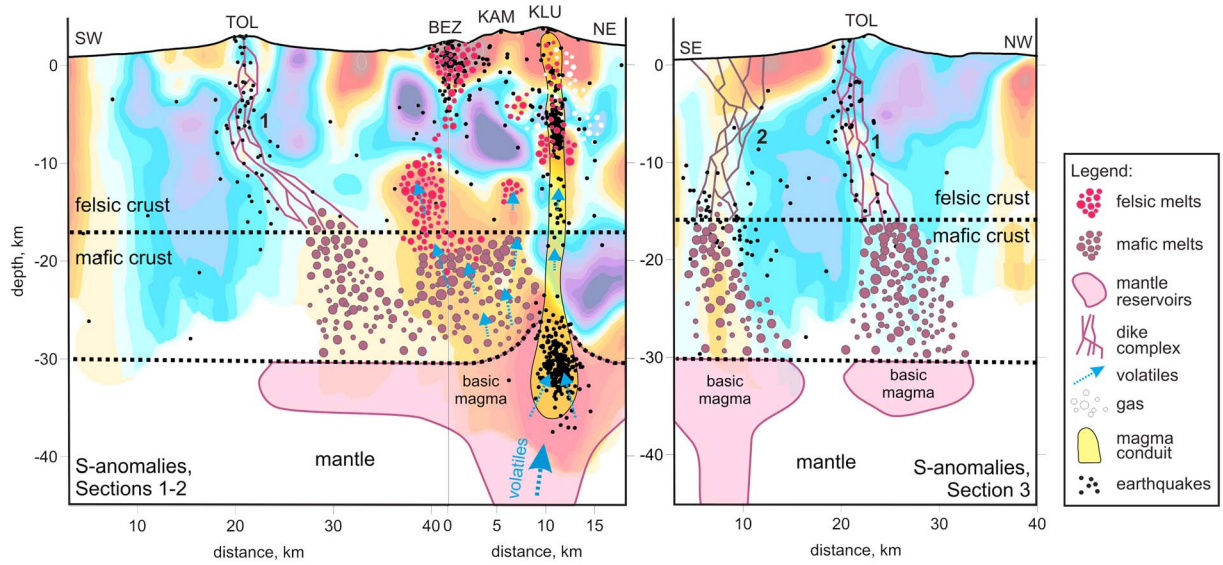

Figure 13. Interpretation of the seismic model. The background is the distribution of *S* wave velocity anomalies in sections 1–3, as in Figure 11. The black dots denote earthquakes.

depth of the Moho may be a result of active mechanical/chemical/thermal processes producing high pressure and stress.

As shown in Figure 14, the seismicity beneath Klyuchevskoy forms a narrow, vertically oriented cluster, which begins at a depth of 30 km and ends at the summit of the volcano. In addition to major seismicity between 25 and 30 km depth, another dense cluster of seismicity is observed at depths from 10 to 5 km, which coincides with the greatest contrast in seismic velocities in the crust. However, the observed linear seismicity does not have any apparent association with the distribution of the main velocity anomalies. We propose that this near-vertical seismicity line represents a narrow conduit bringing molten magma directly from the mantle to the surface; this feature is schematically indicated by the yellow zone in Figures 13 and 14. Lack of

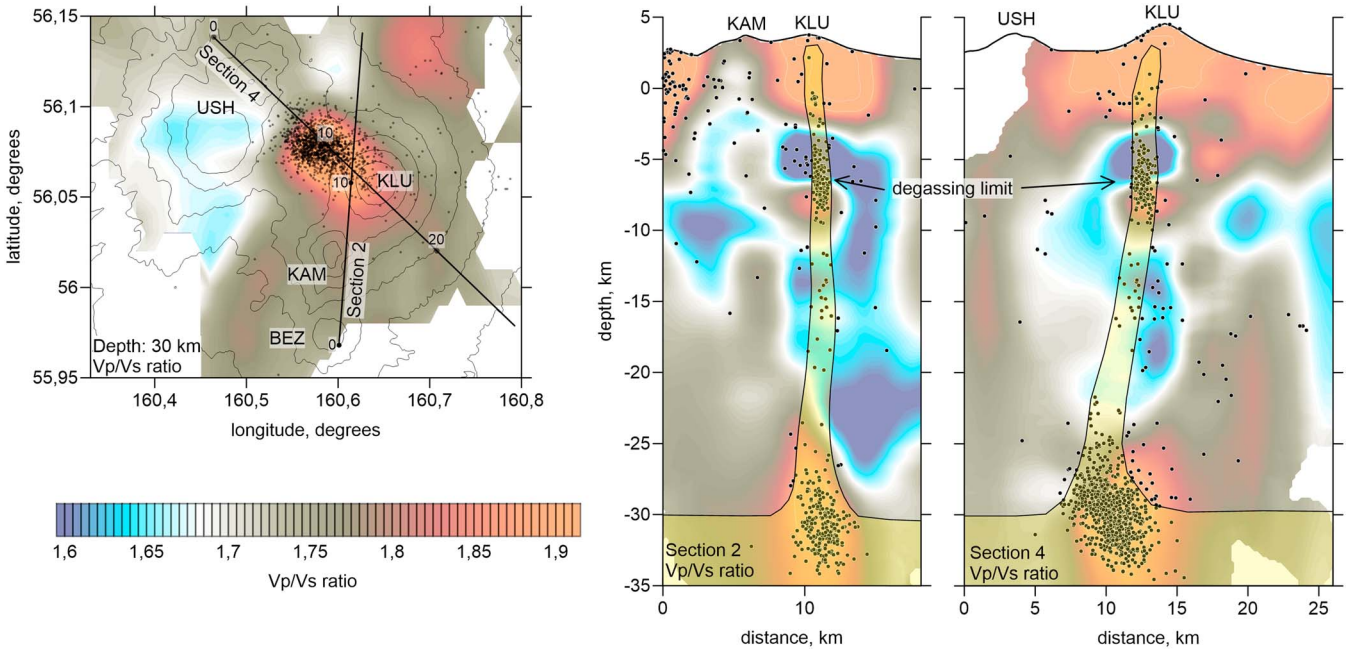

Figure 14. Distributions of *Vp/Vs* ratios at 30 km depth and in two vertical sections in the area of the Klyuchevskoy volcano and a possible interpretation. The magma conduit beneath Klyuchevskoy is schematically depicted with yellow polygons in areas with vertically oriented seismicity (black dots).

association of seismic anomalies with the location of this conduit might be due to insufficient resolution of the tomography inversion to resolve such a narrow pipe.

To explain what drives the mafic magma, which is denser than the felsic rocks in the upper crust, upward, we first propose that the ascent of magma in the conduit pipe is driven by exceptionally high pressure in the reservoir at the bottom of the crust, which is consistent with the extremely strong seismicity at this depth. Second, the mafic magma in the conduit is hot and may be highly saturated with volatiles that decrease its density. At depths between 5 and 10 km, increase in the intensity of seismicity may represent gas release in the conduit caused by decompression of volatiles, as shown, for example, in the modeling results of *Lensky et al.* [2004]. Our tomography model shows neutral *S* and very low *P* wave anomalies with corresponding very low *Vp/Vs* ratios between 7 and 4 km in depth (Figure 14) immediately beneath Klyuchevskoy, which may indicate the presence of the gas phase [e.g., *Takei*, 2002], and this supports this hypothesis. Third, when this magma ascends through the "pipe," it may become enriched with felsic components as it passes through the upper crust, which may decrease the density of the magma. A significant felsic component is detected in the Klyuchevskoy lavas, and its amount varies over time [e.g., *Ozerov et al.*, 1997, 2007]. In our tomography model, the areas with high *Vp/Vs* ratios above 15 km depth may represent zones with partially molten felsic magmas. Some of these zones, located close to the Klyuchevskoy conduit, may provide some of the molten felsic component and change the composition of magmas in the "pipe."

4.2. Bezymianny Volcano—Separation of Light Fractions

The Bezymianny volcano, located 10 km from Klyuchevskoy, is a highly explosive volcano with predominantly dacitic-andesitic compositions [e.g., *Bogoyavlenskaya et al.*, 1991; *Braitseva et al.*, 1991; *Girina*, 2013]. We propose that this volcano is fed from the same mantle reservoir as the Klyuchevskoy volcano. Hot, basic mantle magmas highly saturated with volatiles may be less dense than the rocks of the lower crust and ascend in the form of diapirs. However, these diapirs are not buoyant enough to continue ascending through the lower density felsic upper crust and therefore accumulate at a depth of ~15 km. In this midcrustal magma storage, the lighter felsic fraction may separate and form upper crustal reservoirs. The products of these separations are likely associated with the low-velocity and high *Vp/Vs* ratio anomalies located beneath Bezymianny at depths of 10–15 km. Furthermore, a considerable amount of hot mantle volatiles can easily penetrate upward, which is an efficient method of heat transport. These mantle volatiles may facilitate the melting of felsic rocks in the upper crust to form active reservoirs for present eruptions of Bezymianny.

A similar mechanism was proposed by *Koulakov et al.* [2016b] for the Toba supervolcano, whereby material from the violent, explosive eruptions of this volcano was composed mainly of upper crustal felsic materials. They also identified a large reservoir at the bottom of the crust marked by very low seismic velocity anomalies and high seismicity, similar to those observed beneath the Klyuchevskoy volcano. For Toba, this reservoir served as a powerful source of heat and volatiles, which caused the formation of large crustal magma reservoirs highly contaminated with fluids. In the case of the KGV, the deep reservoir is constantly discharged by the Klyuchevskoy volcano "pipe," which prevents accumulation of the large amounts of fluids required for large-scale eruptions such as those of Toba.

4.3. Tolbachik-Dyke Complex Associated With Fault Zones

During recent eruptions in 1941, 1975, and 2012–2013, the Tolbachik volcano had rather complex eruption regimes [e.g., *Fedotov*, 1984; *Belousov et al.*, 2015; *Churikova et al.*, 2015]. The voluminous basaltic lava flows originated from the summit area and along a fissure that extended ~30 km to the south of the summit along the Tolbachinsky Dol. The composition was mainly basaltic ranged from primitive tholeiitic composition (high MgO) to less primitive alkali-type (high Al basalts) that may coexist within the same eruption. For example, during the 1975–1976 eruption, both tholeiitic and alkali basalts erupted from the Northern and Southern Vents, respectively [*Fedotov*, 1984]. In the crater area of Plosky Tolbachik, alkali basalts dominated, but the eruption of 1941 was presented by the high-magnesium tholeiitic basalts. On the other hand, the lavas of the 2012–2013 eruption, which were also originated in the summit area of Plosky Tolbachik, were similar to the alkali basalts of the Southern Vent [*Churikova et al.*, 2015]. All these geochemical data indicate that lavas in the recent Tolbachik eruptions may originate from different sources and come to the surface through complex pathways.

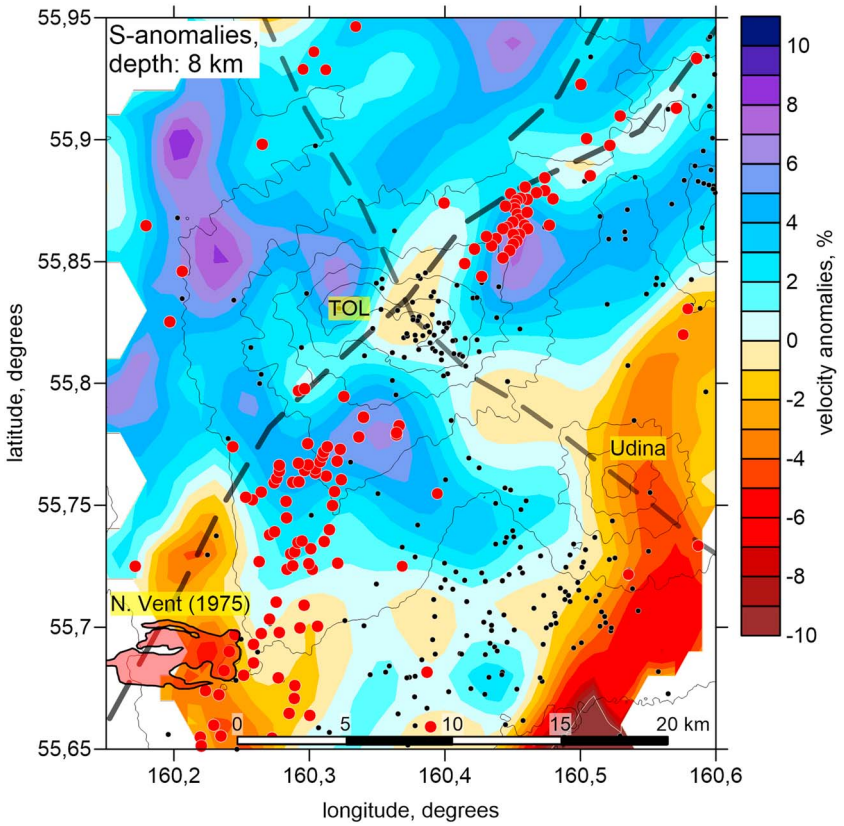

Figure 15. Horizontal section of the *S* wave velocity model at 8 km depth for the area of the Tolbachik volcano (TOL). The dotted lines indicate corrected locations of possible fault zones that cross beneath Tolbachik. The black dots denote seismic epicenters, and the red dots indicate monogenetic cones (as in Figure 1).

Figure 15 shows that the low *S* wave velocity anomalies at 8 km depth delineate linear structures, as indicated with dashed lines that intersect beneath Tolbachik. These anomalies may represent weakened crustal segments associated with two nearly orthogonal fault zones, one of which passes through Klyuchevskoy, Bezymianny, and Tolbachik and another one through Udina volcanoes. These zones appear to be shifted 2–4 km with respect to the lineaments identified from the distributions of volcanic cones (see Figure 1). This shift may be caused by inclination of the fault zone, which originated as a rift-associated structure and thus represents a normal fault with a typical dip angle of approximately 60°. The intersection of the fault zone, which is the weakest part of the crust, may be the main reason for the intensive volcanic activity of Tolbachik. The immense volume of the Plosky and Ostry Tolbachik volcanoes may cause high pressure in the crust. If molten mafic rocks are present in the lower crust, these will be squeezed by lithostatic pressure and move upward along a system of fractures in the fault zone.

Based on our tomography results, we propose that two or three simultaneously active magma sources are present beneath Tolbachik, as shown in Figure 13. One of these magma pathways, marked with"1," may be represented in our tomography result in section 1 as a low *S* wave velocity anomaly that coincides with a linear cluster of seismicity. This magma originates from the same mantle reservoir that feeds Klyuchevskoy and Bezymianny, but from its periphery where the amount of volatiles is much lower.

Another magma pathway, marked with "2," is located to the southeast of Tolbachik (left part of section 3 in Figure 13). Below 15 km depth, to the south of the Udina volcano, a zone with higher *P* and lower *S* wave velocities and a high *Vp/Vs* ratio may indicate intrusions of partially molten magmas. This anomaly coincides with dispersed seismicity at 10–20 km depth. We propose that this anomaly represents another mafic magma reservoir, which may provide additional eruption material to the summit area. In the SW of the map in Figure 15, and at the left border of sections 1 and 2 in Figure 13, we observe a prominent low-velocity anomaly. Although this anomaly is located at the border of the resolved area, synthetic tests indicate that it is

sufficiently robust. This feature may represent another magma source that fed the North Vent and possibly the South Vent in the southern part of the Tolbachinsky Dol. The magmas in this pathway have slightly different properties from those in the pathway "1," as indicated by differences in the compositions of lavas in these areas [e.g., *Churikova et al.*, 2015]. We do not yet have sufficient data to robustly identify the mantle sources of all of these pathways and determine whether they are connected with the Klyuchevskoy source or independent. Another plume may bring the material of the slab according to the concept of magma fingers [*Dobretsov and Kirdyashkin*, 1997, *Tamura et al.*, 2002]; however, the distance between these plumes would be only ~50 km, which is roughly half the expected distance based on the existing shape of subduction beneath Kamchatka.

Note that the different pathways beneath Tolbachik may intersect in some areas and affect each other. Such interaction may explain the existence of different geochemical signatures in lavas corresponding to the same eruption series of Tolbachik.

5. Conclusions

Based on the data from the temporary network deployed in 2014–2015 in the southern part of the Klyuchevskoy group of volcanoes (KGV), we have constructed the first high-resolution model of the crust beneath the Tolbachik volcano area and provided accurate locations of earthquakes. Furthermore, adding data from the Tolbachik and PIRE networks made it possible to enhance the resolution of the tomographic inversion in other parts of the KGV.

In the shallow crust, seismic anomalies show clear segmentation of the main low- and high-velocity blocks with the location of the lineament marked by fissure eruptions in the Tolbachinsky Dol and monogenetic cones to the northeast of Tolbachik. These findings may indicate a regional fault crossing the KGV that is an attractor for the main presently active volcanoes: Tolbachik, Bezymianny, and Klyuchevskoy. Based on the apparent alternation of seismic anomalies at the opposite flanks of this lineament, we propose that there may be lateral displacement indicating a strike-slip mechanism of faulting.

The distributions of seismic anomalies and seismicity in the crust reveal three different feeding mechanisms for the main active volcanoes of the KGV:

1. Beneath the Klyuchevskoy volcano, the seismicity forms a narrow, nearly vertical cluster connecting the deep magma surface at the bottom of the crust with the summit at the surface. The basaltic magma may be delivered to Klyuchevskoy directly from the mantle source through a nearly straight vertical "pipe." This upward movement may be driven by several different mechanisms, such as high pressure in the deep reservoir, volatile degassing due to decompression during ascent, and mixing with lighter felsic rocks in the upper crust.
2. Beneath the Bezymianny volcano, ascending volatile-rich diapirs may originate from the same mantle source as that of Klyuchevskoy but are dispersed. The lighter felsic components gradually separate and continue to ascend to the upper crust. These magmas may form shallow andesitic reservoirs with large amounts of fluids, which may cause the explosive eruptions of Bezymianny.
3. Beneath Tolbachik, we observe two separate pathways marked by seismicity and low *S* wave velocity anomalies. One of these pathways appears to be connected with the marginal part of the Klyuchevskoy deep reservoir, and another seems to originate from an independent mantle source located to the south of Tolbachik. The upward movement of the basaltic magma may be driven by very high lithostatic pressure caused by the immense Tolbachik volcano complex. The squeezed magma follows the weakest zones in the crust, which coincides with regional tectonic faults.

Acknowledgments
We are grateful to Yosuke Aoki, Jeffrey Park, and an anonymous reviewer for their friendly and constructive remarks that helped us to improve the manuscript. This study was supported by the Russian Science Foundation grant 14-17-00430. The authors extend their appreciation to the International Scientific Partnership Program ISPP at King Saud University for funding this research work through ISPP 0044. The field works in 2014 were financially supported by the National Geographic NGS grant 9445-14. Special thanks are given to the truck driver Igor Uteshev and to the helicopter pilot Gennady Kroshkin. The data of this study are available at www.ivan-art.com/science/lotos_tolbachik.zip.

References

Belousov, A., M. Belousova, B. Edwards, A. Volynets, and D. Melnikov (2015), Overview of the precursors and dynamics of the 2012–13 basaltic fissure eruption of Tolbachik volcano, Kamchatka, Russia, *J. Volcanol. Geotherm. Res.*, *307*, 22–37.

Bijwaard, H., W. Spakman, and E. R. Engdahl (1998), Closing the gap between regional and global travel time tomography, *J. Geophys. Res.*, *103*(B12), 30,055–30,078.

Bogoyavlenskaya, G. E., O. A. Braitseva, I. V. Melekestsev, A. P. Maksimov, and B. V. Ivanov (1991), Bezymianny volcano, in *Active Volcanoes of Kamchatka*, vol. 1, pp. 195–197, Nauka, Moscow.

Braitseva, O. A., I. V. Melekestsev, G. E. Bogoyavlenskaya, and A. P. Maksimov (1991), Bezymyannyi: Eruptive history and dynamics, *Volcanol. Seismol.*, *12*, 165–194.

Churikova, T. G., B. N. Gordeychik, B. R. Edwards, V. V. Ponomareva, and E. A. Zelenin (2015), The Tolbachik volcanic massif: A review of the petrology, volcanology and eruption history prior to the 2012–2013 eruption, *J. Volcanol. Geotherm. Res.*, *307*, 3–21.

Dobretsov, N. L., and A. G. Kirdyashkin (1997), Modeling of subduction processes, *Russ. Geol. Geophys.*, *37*(5), 846–857.

Dobretsov, N. L., I. Y. Koulakov, and Y. D. Litasov (2012), Migration paths of magma and fluids and lava compositions in Kamchatka, *Russ. Geol. Geophys.*, *53*, 1253–1275.

Droznin, D. V., and S. Y. Droznina (2011), Interactive DIMAS program for processing seismic signals, *Seism. Instrum.*, *47*, 215–224.

Ermakov, V. A., and A. A. Vazheevskaya (1973), Ostry and Plosky Tolbachik volcanoes [in Russian], *Bull. Volcanol. Stations*, *49*, 43–53.

Fedotov, S. A. (1984), *The 1975–1976 Large Tolbachik Fissure Eruption in Kamchatka* [in Russian], p. 637, Nauka, Moscow.

Flerov, G. B., and A. A. Ovsyannikov (1991), Ushkovsky volcano, in *Active Volcanoes of Kamchatka*, vol. 1, edited by S. A. Fedotov and Y. P. Masurenkov, pp. 164–165, Nauka, Moscow.

Fukao, Y., and M. Obayashi (2013), Subducted slabs stagnant above, penetrating through, and trapped below the 660 km discontinuity, *J. Geophys. Res. Solid Earth*, *118*, 5920–5938, doi:10.1002/2013JB010466.

Girina, O. (2013), Chronology of Bezymianny volcano activity, 1956–2010, *J. Volcanol. Geotherm. Res.*, *263*, 21–40.

Gorbatov, A., V. Kostoglodov, G. Suarez, and E. Gordeev (1997), Seismicity and structure of the Kamchatka subduction zone, *J. Geophys. Res.*, *102*(B8), 17,833–17,898.

Gorbatov, A., J. Dominguez, G. Suarez, V. Kostoglodov, D. Zhao, and E. Gordeev (1999), Tomographic imaging of the P-wave velocity structure beneath the Kamchatka peninsula, *Geophys. J. Int.*, *137*, 269–279.

Gorbatov, A., Y. Fukao, S. Widiyantoro, and E. Gordeev (2001), Seismic evidence for a mantle plume oceanwards of the Kamchatka-Aleutian trench junction, *Geophys. J. Int.*, *146*(2), 282–288.

Gorshkov, G. S. (1959), Gigantic eruption of the volcano Bezymianny, *Bull. Volcanol.*, *20*(1), 77–109.

Grand, S. P. (2002), Mantle shear-wave tomography and the fate of subducted slabs, *Philos. Trans. Roy. Soc. London Ser. A: Math. Phys. Eng. Sci.*, *360*(1800), 2475–2491.

Han, D. H., and M. L. Batzle (2004), Gassmann's equation and fluid-saturation effects on seismic velocities, *Geophysics*, *69*(2), 398–405.

Ivanov, I., I. Koulakov, M. West, A. Jakovlev, E. Gordeev, S. Senyukov, and V. Chebrov (2016), Magma sources beneath the Klyuchevskoy and Bezymianny volcanoes inferred from local earthquake seismic tomography, *J. Volcanol. Geotherm. Res.*, *323*(1), 62–71, doi:10.1016/j.jvolgeores.2016.04.010.

Jiang, G., D. Zhao, and G. Zhang (2009), Seismic tomography of the Pacific slab edge under Kamchatka, *Tectonophysics*, *465*(1), 190–203.

Khrenov, A. P., V. S. Antipin, L. A. Chuvashova, and E. V. Smirnova (1989), Petrochemical and geochemical peculiarity of basalts of the Kluchevskoy volcano, *Volcanol. Seismol.*, *3*, 3–15.

Khrenov, A. P., V. N. Dvigalo, I. T. Kirsanov, S. A. Fedotov, V. I. Gorelchik, and N. A. Zharinov (1991), Klyuchevskoy volcano, in *Active Volcanoes of Kamchatka*, edited by S. A. Fedotov and Y. P. Masurenkov, pp. 146–153, Nauka, Moscow.

Khubunaya, S. A., L. I. Gontovaya, A. V. Sobolev, and I. V. Nizkous (2007), Magma chambers beneath the Klyuchevskoy volcanic group (Kamchatka), *J. Volcanol. Seismol.*, *2*, 98–118.

Koulakov, I. (2009), LOTOS code for local earthquake tomographic inversion: Benchmarks for testing tomographic algorithms, *Bull. Seismol. Soc. Am.*, *99*(1), 194–214, doi:10.1785/0120080013.

Koulakov, I., E. I. Gordeev, N. L. Dobretsov, V. A. Vernikovsky, S. Senyukov, and A. Jakovlev (2011b), Feeding volcanoes of the Kluchevskoy group from the results of local earthquake tomography, *Geophys. Res. Lett.*, *38*, L09305, doi:10.1029/2011GL046957.

Koulakov, I., E. I. Gordeev, N. L. Dobretsov, V. A. Vernikovsky, S. Senyukov, A. Jakovlev, and K. Jaxybulatov (2013), Rapid changes in magma storage beneath the Klyuchevskoy group of volcanoes inferred from time-dependent seismic tomography, *J. Volcanol. Geotherm. Res.*, *263*, 75–91, doi:10.1016/j.jvolgeores.2012.10.014.

Koulakov, I., E. Kukarina, E. I. Gordeev, V. N. Chebrov, and V. A. Vernikovsky (2016a), Magma sources in the mantle wedge beneath the Klyuchevskoy volcano group from seismic tomography inversion, *Russ. Geol. Geophys.*, *57*(1), 82–94, doi:10.1016/j.rgg.2016.01.006.

Koulakov, I., E. Kasatkina, N. M. Shapiro, C. Jaupart, A. Vasilevsky, S. El Khrepy, N. Al-Arifi, and S. Smirnov (2016b), The feeder system of the Toba supervolcano from the slab to the shallow reservoir, *Nat. Commun.*, *7*, 12,228, doi:10.5194/se-7-965-2016.

Koulakov, I. Y., N. L. Dobretsov, N. A. Bushenkova, and A. V. Yakovlev (2011a), Slab shape in subduction zones beneath the Kurile-Kamchatka and Aleutian arcs based on regional tomography results, *Russ. Geol. Geophys.*, *52*, 650–667.

Laverov, N. P. (Ed.) (2005), *Modern and Holocene Volcanism in Russia*, 604 pp., Nauka, Moscow.

Lees, J. M., J. Van Decar, E. Gordeev, A. Ozerov, M. Brandon, J. Park, and V. Levin (2007a), Three dimensional images of the Kamchatka-Pacific plate cusp, in *Volcanism and Subduction: The Kamchatka Region*, edited by J. Eichelberger et al., pp. 65–75, AGU, Washington, D. C.

Lees, J. M., N. Symons, O. Chubarova, V. Gorelchik, and A. Ozerov (2007b), Tomographic images of Kliuchevskoi volcano *P*-wave velocity, in *Volcanism and Subduction: The Kamchatka Region*, edited by J. Eichelberger et al., pp. 293–302, AGU, Washington, D.C.

Lensky, N., V. Lyakhovsky, and O. Navon (2004), Bubble growth during decompression of magma: Experimental and theoretical investigation, *J. Volcanol. Geotherm. Res.*, *129*, 7–22.

Melekestsev, I. V., A. P. Khrenov, and N. N. Kozhemyaka (1991), Tectonic position and general description of volcanoes of northern group and Sredinny Range, in *Active Volcanoes of Kamchatka*, vol. 1, edited by S. A. Fedotov and Y. P. Masurenkov, pp. 74–81, Nauka, Moscow.

Nizkous, I. V., I. A. Sanina, E. Kissling, and L. I. Gontovaya (2006), Velocity properties of the lithosphere in the ocean-continent transition zone in the Kamchatka region from seismic tomography data, *Izv. Phys. Solid Earth*, *42*(4), 286–296.

Nolet, G. (1987), Seismic wave propagation and seismic tomography, in *Seismic Tomography*, edited by G. Nolet, pp. 1–23, Reidel, Dordrecht.

Ozerov, A. Y., A. A. Ariskin, P. Kyle, G. E. Bogoyavlenskaya, and S. F. Karpenko (1997), A petrological–geochemical model for genetic relationships between basaltic and andesitic magmatism of Klyuchevskoi and Bezymiannyi volcanoes, Kamchatka, *Petrology*, *5*, 550–569.

Ozerov, A. Y., P. P. Firstov, and V. A. Gavrilov (2007), Periodicities in the dynamics of eruptions of Klyuchevskoi volcano, Kamchatka, in *Volcanism and Subduction: The Kamchatka Region*, *Geophys. Monogr. Ser.*, vol. 172, edited by Eichelberger et al., pp. 283–291, AGU, Washington, D. C., doi:10.1029/172GM20.

Paige, C. C., and M. A. Saunders (1982), LSQR: An algorithm for sparse linear equations and sparse least squares, *ACM Trans. Math. Softw.*, *8*, 43–71.

Park, J., V. Levin, M. Brandon, J. Lees, V. Peyton, E. Gordeev, and A. Ozerov (2002), A dangling slab, amplified arc volcanism, mantle flow and seismic anisotropy in the Kamchatka plate corner, in *Plate Boundary Zones*, *AGU Geodyn. Ser.*, vol. 30, edited by S. Stein and J. T. Freymueller, pp. 295–324, AGU, Washington, D. C., doi:10.1029/GD030p0295.

Ponomareva, V. V., T. G. Churikova, I. V. Melekestsev, O. A. Braitseva, M. M. Pevzner, and L. D. Sulerzhitsky (2007), Late Pleistocene-Holocene volcanism on the Kamchatka peninsula, Northwest Pacific region, in *Volcanism and Subduction: The Kamchatka Region*, *Geophys. Monogr. Ser.*, vol. 172, edited by J. Eichelberger et al., pp. 165–198, AGU, Washington, D. C., doi:10.1029/172GM15.

Shapiro, M. N., V. A. Ermakov, A. E. Shantser, V. I. Shuldiger, A. I. Khanchuk, and S. V. Vysotsky (1987), *Remarks on the Tectonic Development of Kamchatka*, 248 pp., Nauka, Moscow.

Slavina, L. B., I. A. Garagi, V. I. Gorelchik, B. V. Ivanov, and B. A. Belyankin (2001), Velocity structure and stress-deformation state of the crust in the area of the Kluchevskoy volcano group in Kamchatka, *Volcanol. Seismol.*, *1*, 49–59.

Takei, Y. (2002), Effect of pore geometry on Vp/Vs: From equilibrium geometry to crack, *J. Geophys. Res.*, *107*(B2), 2043, doi:10.1029/2001JB000522.

Tamura, Y., Y. Tatsumi, D. Zhao, Y. Kido, and H. Shukuno (2002), Hot fingers in the mantle wedge: New insights into magma genesis in subduction zones, *Earth Planet. Sci. Lett.*, *197*, 105–116.

Thelen, W., M. West, and S. Senyukov (2010), Seismic characterization of the fall 2007 eruptive sequence at Bezymianny volcano, *Russia. J. Volcanol. Geotherm. Res.*, *194*, 201–213.

Turner, S., P. Izbekov, and C. Langmuir (2013), The magma plumbing system of Bezymianny volcano: Insights from a 54 year time series of trace element whole-rock geochemistry and amphibole compositions, *J. Volcanol. Geotherm. Res.*, *263*, 108–121.

Um, J., and C. H. Thurber (1987), A fast algorithm for two-point seismic ray tracing, *Bull. Seismol. Soc. Am.*, *77*, 972–986.

Yogodzinski, G. M., J. M. Lees, T. G. Churikova, F. Dorendorf, G. Wöerner, and O. N. Volynets (2001), Geochemical evidence for the melting of subducting oceanic lithosphere at plate edges, *Nature*, *409*(6819), 500–504.

Watanabe, T. (1993), Effects of water and melt on seismic velocities and their application to characterization of seismic reflectors, *Geophys. Res. Lett.*, *20*(24), 2933–2936.

West, M. E. (2013), Recent eruptions at Bezymianny volcano: A seismological comparison, *J. Volcanol. Geotherm. Res.*, *263*, 42–57, doi:10.1016/j.jvolgeores.2012.12.015.

Zhao, D. (2004), Global tomographic images of mantle plumes and subducting slabs: Insight into deep Earth dynamics, *Phys. Earth Planet. In.*, *146*(1), 3–34.